VYSOKÉ UČENÍ TECHNICKÉ V BRNĚ

BRNO UNIVERSITY OF TECHNOLOGY

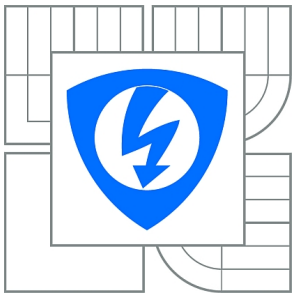

FAKULTA ELEKTROTECHNIKY A KOMUNIKAČNÍCH TECHNOLOGIÍ

ÚSTAV BIOMEDICÍNSKÉHO INŽENÝRSTVÍ

FACULTY OF ELECTRICAL ENGINEERING AND COMMUNICATION

DEPARTMENT OF BIOMEDICAL ENGINEERING

SYNTHESIS OF COLLOIDAL GOLD NANORODS FOR BIOMEDICAL APPLICATIONS

SYNTÉZA KOLOIDNÍCH ZLATÝCH NANOTYČINEK PRO BIOMEDICÍNSKÉ APLIKACE

DIPLOMOVÁ PRÁCE

MASTER'S THESIS

AUTOR PRÁCE — Bc. JIŘINA VALKOVIČOVÁ

AUTHOR

VEDOUCÍ PRÁCE — Ing. JANA DRBOHLAVOVÁ, Ph.D.

SUPERVISOR

BRNO 2014

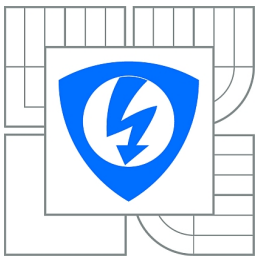

VYSOKÉ UČENÍ TECHNICKÉ V BRNĚ

Fakulta elektrotechniky a komunikačních technologií

Ústav biomedicínského inženýrství

Diplomová práce

magisterský navazující studijní obor
Biomedicínské inženýrství a bioinformatika

Studentka: Bc. Jiřina Valkovičová ***ID:*** 125087
Ročník: 2 ***Akademický rok:*** 2013/2014

NÁZEV TÉMATU:

Syntéza koloidních zlatých nanotyčinek pro biomedicínské aplikace

POKYNY PRO VYPRACOVÁNÍ:

1) Prostudujte metody přípravy zlatých nanotyčinek v roztoku pro využití v biomedicínských aplikacích, zejména pro termální terapii. 2) Proveďte laboratorní syntézy zlatých koloidních nanotyčinek. 3) Analyzujte jejich chemické a fyzikální vlastnosti, eprodukovatelnost, stabilitu, případně cytotoxicitu. 4) Podrobně diskutujte výsledky a porovnejte je s publikovanými daty. Zjištěná fakta shrňte do hodnotného závěru. 5) Naznačte směry dalšího výzkumu v dané oblasti s ohledem na Vaši práci.

DOPORUČENÁ LITERATURA:

[1] HUANG, X. H. et al. Cancer cell imaging and photothermal therapy in the near-infrared region by using gold nanorods. Journal of the American Chemical Society, 2006, vol. 128, no. 6, pp. 2115-2120. ISSN 0002-7863.
[2] ALKILANY, A. M. et al. Gold nanorods: Their potential for photothermal therapeutics and drug delivery, tempered by the complexity of their biological interactions. Advanced Drug Delivery Reviews, 2012, vol. 64, no. 2, pp. 190-199. ISSN 0169-409X.

Termín zadání: 10.2.2014 ***Termín odevzdání:*** 23.5.2014

Vedoucí práce: Ing. Jana Drbohlavová, Ph.D.
Konzultanti diplomové práce:

prof. Ing. Ivo Provazník, Ph.D.
Předseda oborové rady

UPOZORNĚNÍ:

SIX research centre
sensor, information and communication systems

Faculty of Electrical Engineering
and Communication

Brno University of Technology
Technicka 12, CZ-61600 Brno, Czech Republic

http://www.six.feec.vutbr.cz

Výzkum popsaný v této diplomové práci byl realizován v laboratořích podpořených z projektu SIX; registrační číslo CZ.1.05/2.1.00/03.0072, operační program Výzkum a vývoj pro inovace.

MINISTERSTVO ŠKOLSTVÍ, MLÁDEŽE A TĚLOVÝCHOVY

EVROPSKÁ UNIE
EVROPSKÝ FOND PRO REGIONÁLNÍ ROZVOJ
INVESTICE DO VAŠÍ BUDOUCNOSTI

2007–13
OP Výzkum a vývoj pro inovace

Abstrakt

Diplomová práce se zabývá výrobou a využitím zlatých koloidních nanotyčinek v biomedicínských aplikacích. Konkrétně se zaměřuje na tři základní funkce nanočástic v analýze - transportní, separační a především zobrazovací.

V části o využití nanočástic pro zobrazování je hlavní zájem věnován zejména povrchové plazmonové rezonanci zlatých nantyčinek. Dále je práce zaměřena na využití nanotyčinek pro termální terapii.

Následující část je věnována vhodným modifikacím povrchu, hlavně za účelem zmírnění toxicity částic.

Závěrem teoretické části jsou způsoby přípravy zlatých koloidních nanotyčinek a techniky jejich následné analýzy.

V navazující experimetální části jsou uvedeny postupy, podmínky a výsledky provedených pokusů.

Abstract

The diploma thesis discusses the use and the preparation of gold colloid nanorods in biomedical applications. In particular, three elementary functions of nanoparticles in the analysis - transport, separation and imaging.

In the section of nanoparticles usage in imaging, the main interest is the application of surface plasmon resonance. Futher part is focus on the gold nanorods application in thermal therapy.

The following section is devoted to the suitable techniques for nanorods surface modification for the purpose of alleviate the toxicity.

The concept for preparation and analyzation of gold colloid nanorods is mentioned at the end of the theoretical section.

The following laboratory section contains methods, conditions and the results description of already performed experiments.

Klíčová slova

Zlato, nanotyčinky, koloidní roztok, povrchový plazmon, CTAB, photothermal therapy, PEG, MTT assay

Key words

Gold, nanorods, colloid solution, surface plasmon, CTAB, photothermal therapy, PEG, MTT assay

Prohlášení

Prohlašuji, že diplomovou práci na téma Syntéza koloidních zlatých nanotyčinek pro biomedicínskou aplikaci jsem vypracovala samostatně pod vedením vedoucího diplomové práce a s použitím odborné literatury a dalších informačních zdrojů, které jsou všechny citovány v práci a uvedeny v seznamu literatury na konci práce.

Jako autorka uvedené diplomové práce dále prohlašuji, že v souvislosti s vytvořením této práce jsem neporušil autorská práva třetích osob, zejména jsem nezasáhl nedovoleným způsobem do cizích autorských práv osobnostních a jsem si plně vědom následků porušení ustanovení § 11 a následujících autorského zákona č. 121/2000 Sb., včetně možných trestněprávních důsledků vyplývajících z ustanovení § 152 trestního zákona č. 140/1961 Sb.

V Brně dne 23. května 2014 .....

podpis autorky

Poděkování

Děkuji své vedoucí Ing. Janě Drbohlavové, Ph. D. za účinnou metodickou, pedagogickou a odbornou pomoc a další cenné rady při zpracování. Zejména však za její trpělivost a neustálou maximální podporu. Dále děkuji Radimovi Hrdému, Marianovi Marikovi, Naděždě Pizúrové, Vojtěch Enevovi a Michalu Kalinovi za jejich pomoc při vyhodnocování výsledků. V závěru bych ráda poděkovala svým rodičům, zejména své mamince za zázemí a trpělivou podporu za všech okolností.

V Brně dne 23. května 2014 .....

podpis autorky

VALKOVIČOVÁ, J. *Syntéza koloidních zlatých nanotyčinek pro biomedicínské aplikace.* Brno: Vysoké učení technické v Brně, Fakulta elektrotechniky a komunikačních technologií, 2014. 78 s. Vedoucí diplomové práce doc. Ing. Jana Drbohlavová, Ph.D.

Content

Introduction

Cancer, tumors, chemotherapy – the attention gained by this phenomenon indicates how important and grave topic it is. That is the reason why this issue has got public, mainly scientists interests all around the word. Nanoparticles (NPs) are considered as one of the most promising agents for cancer therapy. They are being investigated as drug carriers, photothermal agents, contrast agents and radiosensitisers. Metallic NPs, particulary gold nanorods (AuNRs), have a lot of specific and unique properties, which make a perfect candidate for cancer therapy out of them. There are several problems that are necessary to be solved in the preparation of AuNRs. A big task is to prepare the biocompatible nanostructures which are all uniform and reproducible in a given size. Nowadays, the increasing trend to be careful to the environment spreads to the research in the field of nanotechnology. The development of alternative eco-friendly methods, which means simple, cost-effective and so called green procedures, is one of the major research priorities.

The aim of the thesis is to produce a colloidal AuNRs solution, which will be used for biomedical applications, specifically for photothermal therapy. The unique properties, the preparation technique and the possible characterization of AuNRs will be described in this work.

1. Gold Nanoparticles

While using nanoparticles, it is necessary to solve several problems. The nanostructures need to be prepared so that they are all uniform and reproducible right at the beginning. Their additional modification follows in order to increase their specificity and eventually confirm their AuNPs functionality. A big problem is stability of colloid solution, specifically kinetic and aggregation stability. Colloid NPs solution is formed by NPs dispersion in fluid. Water is usually used as a fluid. Kinetic stability is assured if the concentration distribution of colloids is constant in solution independently on gravity field. By aggregation stability is meant that the dispersed phase size distribution of NPs is constant. Colloid NPs tend to be kinetically unstable and they form aggregates and sediments [1].

1.1. Different shapes of gold nanoparticles

Gold nanocubes (AuNCs), nanorods (AuNRs), nanospeheres (AuNSs), etc. are structures which may vary from one to another not only in the shape but also in the preparation and final use (Figure 1) [2]. At the same time they have one thing in common - they are all particles whose dimensions are in the nanometer range. The shape, which may affect their final chemical and physical properties and thus their application, depends mainly on the method of preparation.

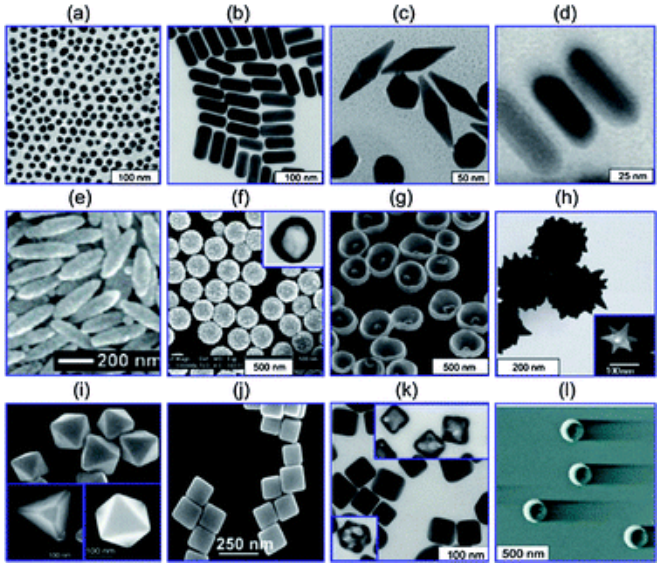

Figure 1 Different shapes of gold nanoparticles: a) nanospheres, b) nanorods, c) nanobipyramids, d) nanorods, e) nanoelliptical disks, f) nanospheres, g) nanoshells, h) nanostars, i) trigonal nanobipyramids and rhombic nanododecahedra, j) nanocubes, k) nanocages l) nanotoroids [2]

The color of AuNPs colloidal dispersion changes from red to blue depending upon the NPs shape and size (Figure 2) [3]. While the NRs solution is red at the highest apect ratio (AR) and blue at the lowest, nanoshells appears as green at the lowest and red at the highest shell thickness and nanocages solution changes its colour due to the percentage representation of gold in the solution.

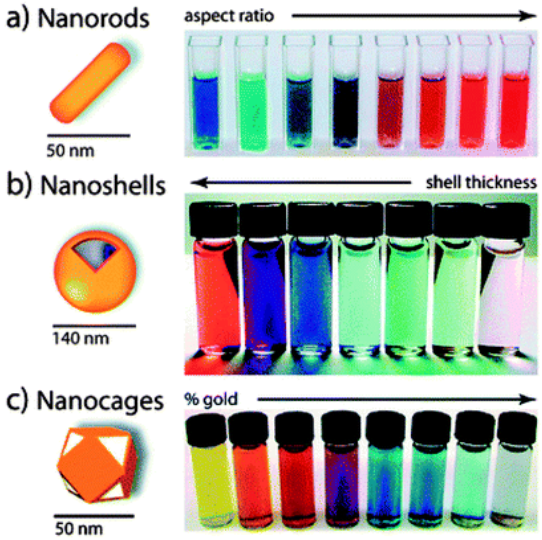

Figure 2 AuNPs colloidal dispersion of various color depending on different sizes and shapes [3]: a) nanorods; b) nanoshells, c) nanocages

The anisotropic (nonspherical) metal nanostructures like AuNRs are very appreciated for their shape-dependent optical properties. Due to the different absorption of visible light along length and width of NRs, a multiple plasmon bands arise in the UV-vis-NIR absorption spectrum of AuNRs solution (for detailed information, see chapter 2.4.1 Plasmon resonance of gold nanorods) [4]. The plasmon peak position varies with different AR. Small changes in the AR of AuNRs cause dramatic changes in the transmitted colors (Figure 3) [5]. The plasmon bands position can be also changed by AuNPs aggregation [6].

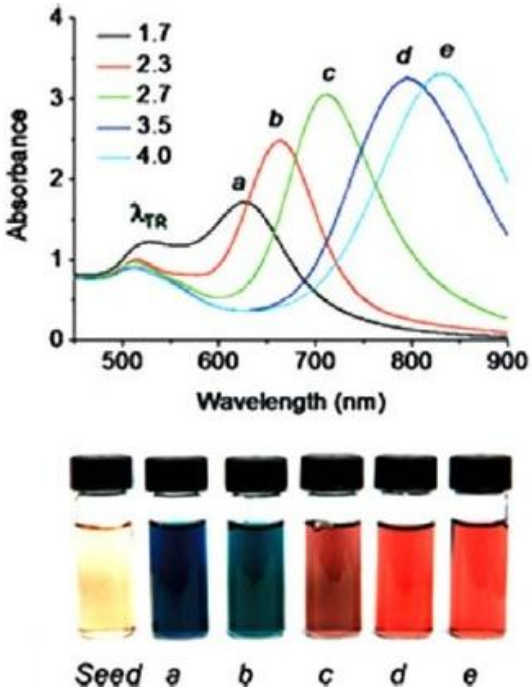

Figure 3 Plasmon peak position and transmitted colors of caused by different ARs of AuNRs[5]

2. Gold nanorods in biomedical applications

AuNRs have an extensive spectrum of biomedical applications, from macromolecules separation to targeted drugs delivery. A big advantage is AuNPs tunable size and shape, which can be made by small and easy changes in synthetic protocols and which can make big differences in final properties [6,7]. But one of NPs disadvantages complicated AuNRs use is their frequent cellular toxicity. It negatively affects the application, mainly in medicine [8]. The problem can be solved by coating nanostructures with a substance compatible with the human body, see chapter Modification and functionalization of gold nanorods.

2.1. Gold nanorods in biomedical separation

AuNRs can be used as affinity templates for the efficient separation of macromolecules, especially of proteins. Their additional modification is mostly a prerequisite for increasing their specificity [9]. Gold is a good choice for protein separation due to its strong affinity for hydrogen and -SH and -NH_2 groups, which is present in the cystein thiol group of natural proteins [10].

2.2. Gold nanorods in optical applications

In optical methods, the AuNPs are used mainly for the purpose of contrast enhancement due to the gold electron density which induces a strong X-ray attenuation and due to its surface plasmon resonance responsible for an enhancement of the local electric field and Raman scattering (used in Surface Enhanced Raman spectroscopy - SERS) effect. That is why the AuNRs are an ideal candidate as a contrast agent for imaging applications [2,11]. Compared with the atomic number and electron density of gold (79 and 19.32 g/cm^3), the current predominant CT contrast agents as iodine molecules (53 and 4.9 g/cm^3) are much lower, consequently AuNRs can induce a strong X-ray attenuation. It is one of the reasons why to use AuNRs in CT applications [12].

2.3. Gold nanorods as a transport medium

In general, most of the nanoparticle properties are used mainly in the drug transport to the specific destination. It is necessary to ensure the maximum drug effectiveness in the site of the disease together with minimal side effects. The drugs need to be reliablely delivered to the area where we need it most, with the greatest therapeutic effect. This is the main reason why to use nanoparticle carriers. They are able of so-called targeted therapy - the active substance delivered straight to outbreaks of disease. The drug effectiveness will naturally increase when the active substance act directly in the cell space [13]. Therefore another requirement is no substance delivery to a cell, but directly into the cell, thus the transport through the cell membrane (Figure 4). The exact transport allows to reduce the dose, without changing the final effect.

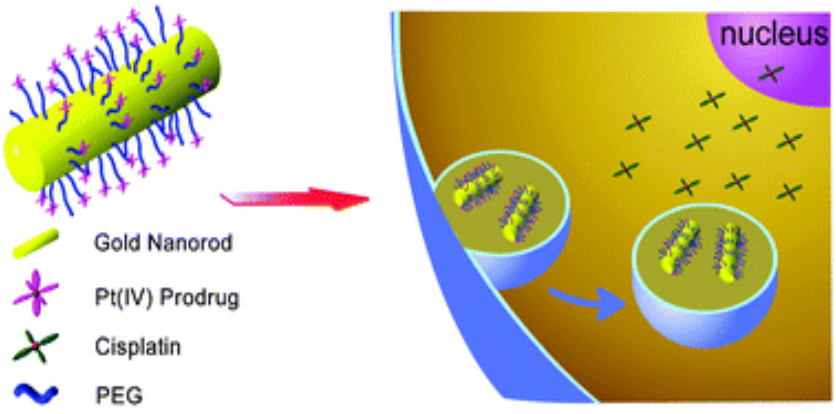

Figure 4 PEGylated gold nanorods conjugated with Pt(IV) prodrug as a drug delivery system used in targeted therapy, i.e. cancer therapy [13]

2.4. Gold nanorods in surface plasmon resonance applications

2.4.1. Plasmon resonance of gold nanorods

One of the advantages of gold, as an electric conductor, is a large number of free electrons in the crystal lattice. These free electrons accumulate on the surface at the interface with air, which holds the role of insulation. It causes fluctuations in surface electrical charge. The photoluminescence properties are increased by the light energy. Light rays cause excitations of surface electrons bound to the interface - so called surface plasmon [14]. Light can be strongly absorbed especially by AuNRs. The conduction band electrons are excited in the gold when AuNRs are illuminated at the proper optical frequencies. It results in a resonant coherent oscillation of these electrons - the localized surface plasmon resonance (LSPR) phenomenon [7].

As mentioned before, the anisotropic NPs show much better optical properties in the form of multiple plasmon bands, unlike the spherical NPs. One band is formed for the transverse plasmon and the other one for the longitudinal plasmon. The longitudinal plasmon band is formed due to the absorption of visible light along the length of the nanorod, contrary to the transverse plasmon band along the width of the nanorod. It follows that the more red-shifted longitudinal plasmon band is formed by the AuNRs with larger AR (Figure 5) [15].

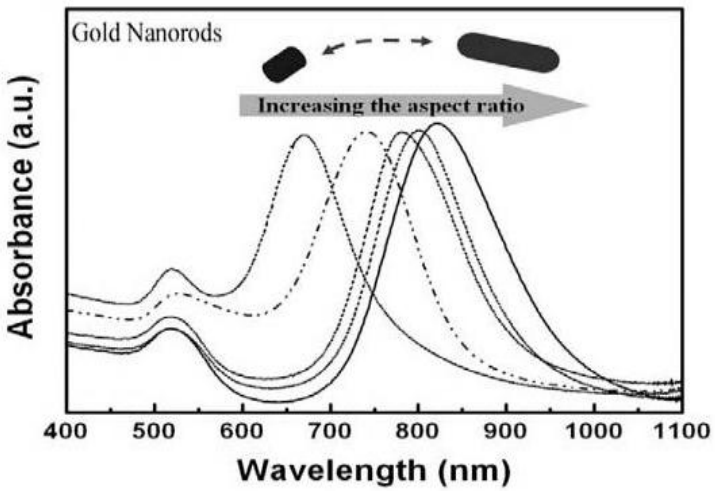

Figure 5 AuNRs UV-visible absoption spectra dependence on the NRs aspect-ration [16]

There are two basic steps of SPR process - excitation and relaxation [17]. The electromagnetic field generated during the process of SPR excitation gets scientists' attention. The field can interact with chemical species and materials. This fact is used for enhancing scattering spectra of chemical species adsorbed onto AuNPs [18,19]. The heat releasing during the relaxation process is a typical feature that brings a lot of advantages [20].

SPR depends on two basic issues - the properties of the excitation beam and the NPs characteristics. Final properties can be influenced by polarization, wavelength, and angle of the excitation ray incidence but also by structure, size and shape of NPs [11,21]. The energy of longitudinal plasmon depends mainly on the AR of AuNRs. Linear dependence is proven between the AuNRs with AR between 2–5 and LSPR [22]. However, the dimensions (length and width) are very important control elements in absorption vs scattering efficiency, due to the dependence of the efficiency on the volume [23]. Ali et al. have demonstrated that NRs of larger diameter have larger extinction coefficient than the small NRs [22]. It follows that the small NPs are better in medical applications for example for the improvement of efficiency in photo-thermal therapy, whilst the bigger NPs have better results in optical imaging. Human body contains from 55% to 78% of water, depending on body size. Based on the wavelength criterion, the "water window" where aqueous tissue absorbs relatively little light, i.e. in the range of 700–1200 nm, is considered to be the best spectral region for imaging and therapy. That is why the surface plasmon absorption around 900 nm is required - this wavelength is safe for a human body. This is the reason why AuNRs with AR below 10 are used for this kind of medical applications [24].

2.4.2. Application of gold nanorods surface plasmon resonance

SPR of AuNRs is mainly used in sensing applications, plasmon enhanced spectroscopies, biomedical imaging and photothermal therapy for cancer.

Strongly enhanced electric near-field generated by LSPR localized at the nanoparticle surface forms the basis of the electromagnetic SERS [25]. SERS is a spectroscopic method for detection of molecular vibrations on or near metallic surfaces. Supporting plasmonic excitation is a necessity. SERS technique is used for chemical or biological sensing. The method is very sensitive so single-molecule could be detected [26]. Zijlstra and col. investigated the optical sensitivity of single non-absorbing molecules detection using the AuNRs SPR. They found out that the binding of the single analyte molecules to the single AuNR functionalized with biotin induced a longitudinal SPR redshift [27].

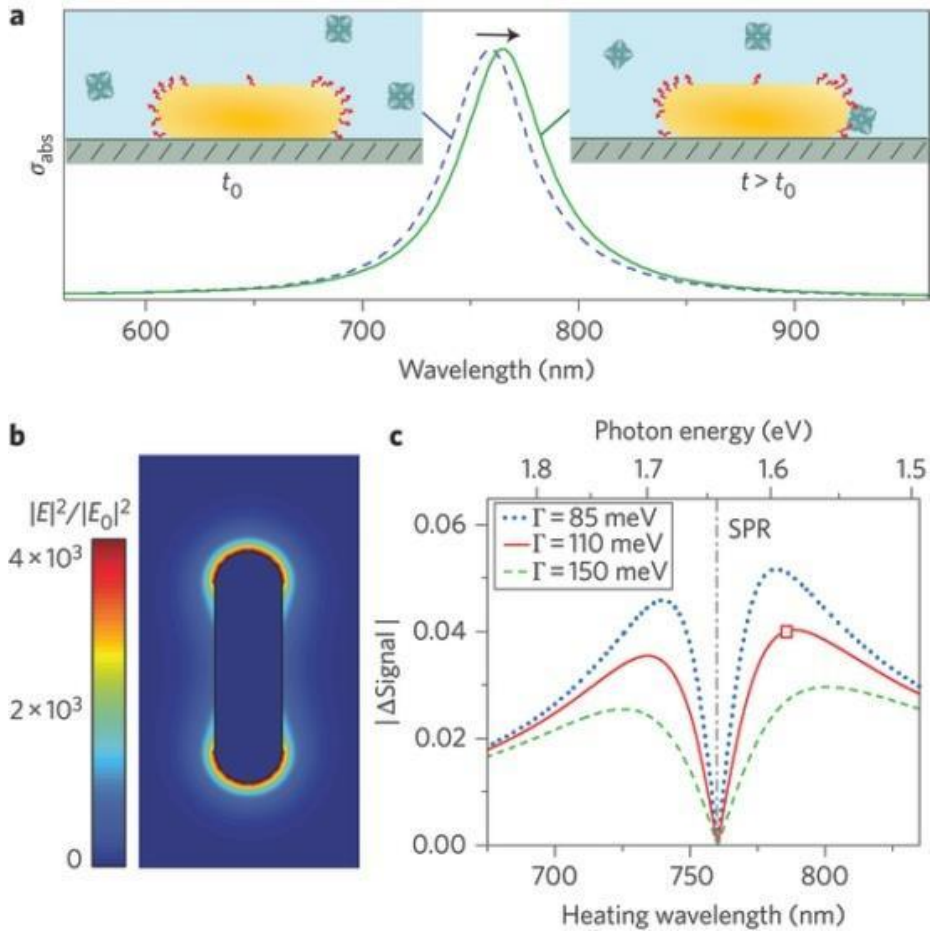

Figure 6 SERS: (a) AuNRs functionalized with biotin, (b) the intensity of modified AuNR, (c) signal intensity changes in UV-VIS spectrum caused by binding analyt molecule [27]

AuNRs showed a strong resonant enhancement of fluorescence emission by the longitudinal LSPR, so they could be used also as the optical fluorescence sensor [11].

2.5. Gold nanorods in photothermal therapy

Cancer, a cruel disease which is one of the most feared causes of death all around the word. There are various therapeutic strategies such as radiation therapy, surgery, chemotherapy etc. which have usually limited efficacy. Photothermal therapy shows a potential as a relatively new approach in cancer treatment. The application of heat to destroy the specific cancer cells is proposed as an encouraging approach in optimizing cancer therapy. The method is very appreciate because of non-invasive targeted character. Specific biological tissues are exposed to high temperature to promote protein denaturation together with membrane disruption leading to cell necrosis [16].

Due to unique photophysical properties, which can be modified by size changes, AuNRs are considered as prime candidate agents for the photothermal cancer treatment. It is necessary to ensure the maximum effectiveness in the site of tumor with the minimum of surrounding tissue stress and minimal side effects in the cancer therapy [28]. The cell death might be induced in the specific area of body in the best case (Figure 7).

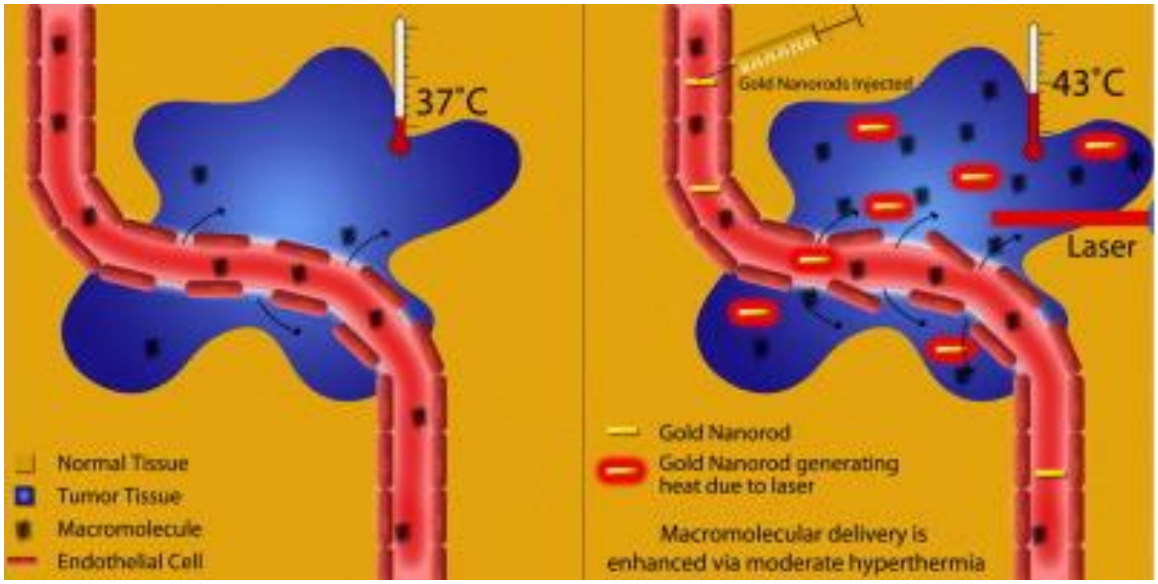

Figure 7 Targeted photothermal cancer therapy, the temperature before the application of AuNRs (left) and after (right) [28]

It is necessary to have an external source of energy during the NPs-assisted photothermal therapy. There is a lot of method how to excite NPs based on the type of external source, for example combination of plasmon-resonant NPs with extrenal magnetic field or with near infrared (NIR) laser.

In the first case, the tumor is destroyed by the heat generated by the effect of variable external magnetic field [29]. The effect is dependent not only on magnetic field size and strength, but also on the speed of blood circulation and the physical and chemical nanoparticle properties. The particles are synthesized in very small sizes ensuring their superparamagnetism. Due to this feature it is guaranteed that the nanoparticles are magnetic only under the influence of the external magnetic field. This ability prevents the nanoparticle aggregation after the removal form the external magnetic field.

In the second case, AuNRs with plasmon absorbance in the NIR can be targeted to tumors *in vivo*. LPSR is used in this kind of method. The AuNRs are irradiated with

electromagnetic radiation at the frequency which matches to the material characteristic resonant frequency. Consequently, all free electrons within the conduction band oscillate with the frequency of the radiation [16]. After AuNRs absorb energy, the energy is quickly transferred through nonradiative relaxation into heat and accompanied effects [30]. The light transformation into heat in nanoscale region could be studied using ultrafast dynamic techniques and computational model [31,32].

Huang and col. have reported that the energy needed to cause the destruction of cancer cells was dependent on the AuNRs uptake quantity in the cells [33]. In general, the NRs are ingested through endocytosis into the cell cytoplasm. There, they are trapped in endosomes, or after several hours in lysosomes, where they are collected into larger clusters (Figure 8).

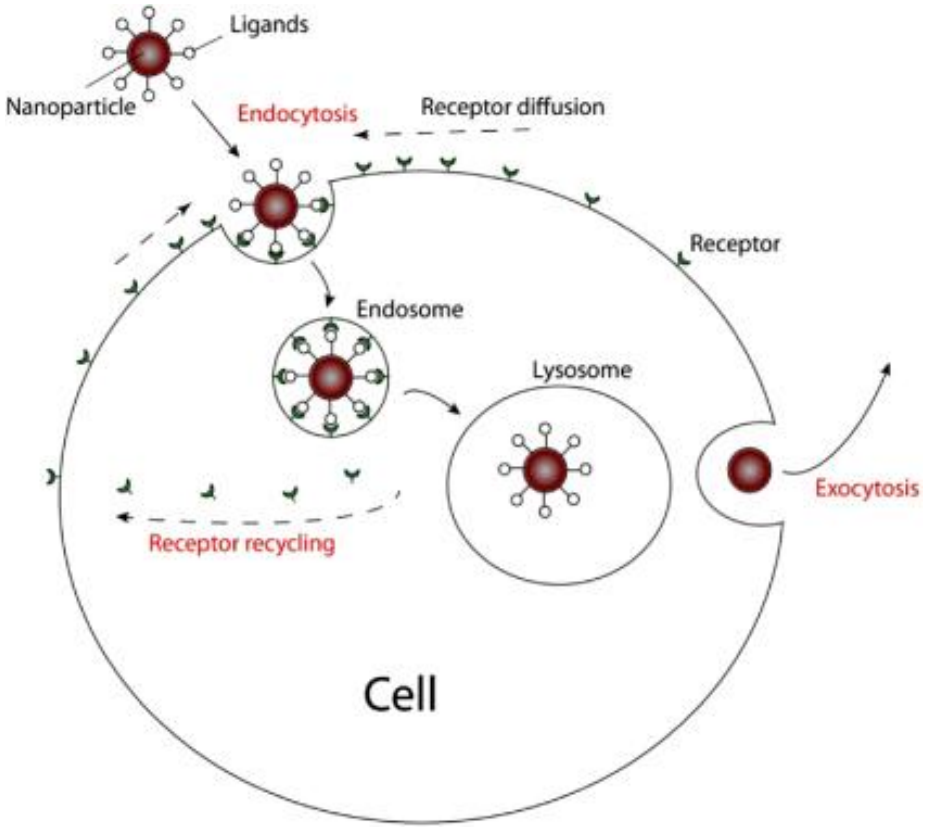

Figure 8 AuNPs uptake into the cell [34]

Zharov et al. have demonstrated that this process of aggregation increases the efficiency of the laser-induced photothermolysis [30]. Okuno and col. have found out that AuNRs were accumulated in the tumor during 24 hours after vein injection and that irradiation with NIR laser light in combination with AuNRs demonstrably elevated tumor temperature. The tumor growth was suppressed more in AuNRs presence than with irradiation alone [35]. The tumor

temperature reached 46 °C for laser irradiation alone, and approximately 51 °C for laser irradiation with AuNRs (either local or systemic). There was also studied the effect on tumor combining local and systemic AuNRs delivery with NIR irradiation - the local AuNRs delivery was slightly better in comparsion with systemic delivery (Figure 9).

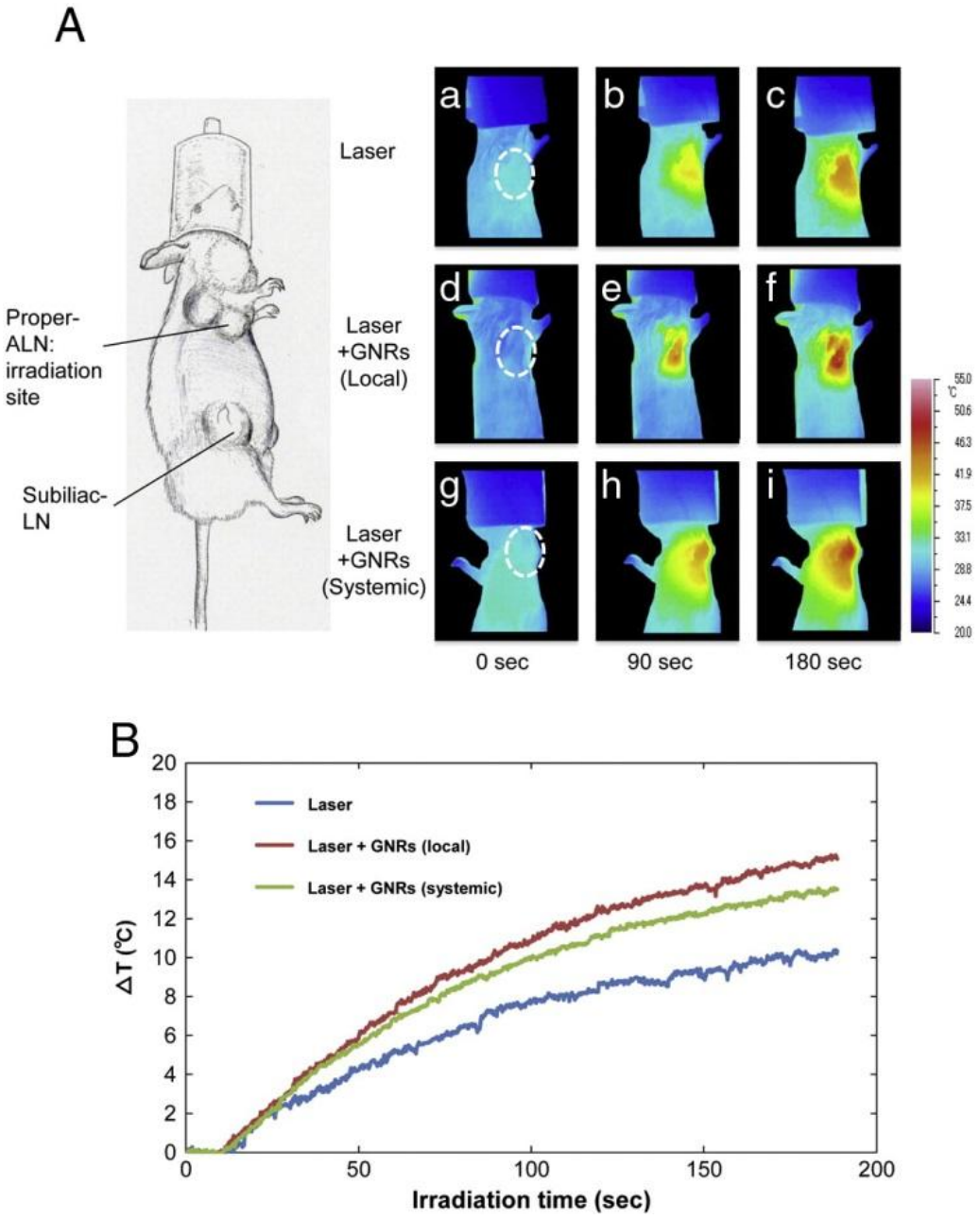

Figure 9 Laser irradiation of tumor: A. Anatomical and thermographic images of tumors, irradiated (a, b, c): laser light alone; (d, e, f): laser light with local GNR delivery; (g, h, i): laser light with systemic GNR delivery. (a, d, g): irradiation time 0 s; (b, e, h): irradiation time 90 s; (c, f, i): irradiation time 180 s. [35]

The heat released by AuNPs after the excitation by NIR laser into the tumor environment could cause the rupture of tumor cell membranes and subsequent death [36]. NRs with low AR and with the same plasmon resonance at NIR are used not only as therapy agents, but for imaging as well [33]. This ability to convert photon energy to heat with high efficiency in combination with strong two-photon photoluminescence make AuNRs an excellent candidate to be used in phototermal therapy, as theranostic anticancer agents (NPs that assist in both, the therapy and diagnosis) and one of the best options of cancer treatment compared with the traditional chemotherapy [16,37,38].

3. Preparation of gold nanorods

There are several problems that are necessary to be solved in the preparation of AuNRs. Perhaps the most important thing is to create the nanostructures which are all uniform and reproducible in a given size.

There are two basic forms of NRs - deposited and colloidal NRs. The deposited form means that NRs are immobilized on solid substrate. Different techniques have been used for NRs anchoring, for example electrodeposition methods which will be mentioned below. The colloidal NRs are very appreciated for their capability to generate a longitudinal surface plasmon [4].

3.1. Hard-template synthesis - Electrochemical methods

The first established synthesis of deposited AuNRs was performed by electrochemical reduction of gold ions. The NPs were prepared through porous alumina template or polycarbonate membrane for the shape control in the presence of surfactant (often cetyltrimethylammonium bromid, CTAB) [21]. These alkyl bromide salts were chosen because of their efficiency as electrolytes. It has been discovered later that CTAB is influential in directing the growth because of its ability to form cylindrical micelles above its second critical micelle concentration [4]. This capability is crucial for another way how to prepare AuNRs – electrochemical reduction using surfactant mixtures as a soft template.

The electrochemical methods have numerous advantages. One of them is undoubtedly control over the length, diameter and wall thickness of nanoparticles. The final form of NPs is influenced by various factors such as the shape of the nanopores or galvanostatic conditions.

3.2. Wet chemistry method - Seeded growth synhesis

This kind of AuNRs synthesis is one of the most popular and used methods nowadays. These techniques are based on addition of small citrate-stabilized AuNPs representing seed solution to series of growth solutions. Growth solution usually contains gold salt, surfactant, and reducing agent. The final NPs AR decrease with increasing size of the seed. The AR dispersity is also influenced by the surface charge of the seed. Ascorbic acid which is usually used as reducing agent in many protocols reduces gold(I) to gold(0) [39]. The final AuNRs are obtained by various processes. Three basic methods will be mentioned in this thesis.

The first one is three-steps seeded growth synhesis which is based on repetitive addition of mixture of citrate-stabilized seed and growth solutions to a new growth solution. AuNRs with AR between 10 and 25 are prepared via this technique [40].

The second approach of AuNRs preparation is one-step silver-assisted seeded growth synhesis. As a seed solution, the procedure utilizes smaller AuNPs stabilized with cetyltrimethylammonium bromide (CTAB), rather than citrate. The growth solution contains a small amount of silver nitrate which is the component controling the final ARs. The NRs ARs can be increased by increasing the silver concentration [41]. Combination of silver and bromid alters the shape of CTAB micelles. AuNRs with ARs between 8−20 nm are synthesized by this method [4].

The last third technique is described by Jana et al., who are the main initiators of sedless silver-assisted AuNRs growth. The authors used the standard silver-assisted seeded growth method with one difference: they generated the seed solution *in situ* by the addition of a small amount of strong reducing agent - sodium borohydride. AuNRs with ARs between 2 and 5 dependent on the concentration of sodium borohydride have been prepared by the method [21]. These AuNRs p have smaller dimension than AuNRs prepared by one-step silver-assisted seeded growth synhesis. The fact is very important especially because these small NPs have AR-dependent plasmon absorbances as larger NPs, but scatter light less strongly than the larger NPs [17].

The development of alternative eco-friendly methods using phototrophic microorganisms, as plants or algae extracts, fruits extracts or vitamins which make nanoparticles syntheses „greener“ is investigated extremely [42].

Nadagouda et al. reported green chemistry approach in the AuNRs preparation using oxidized vitamin B2 as reducing and capping agent for Au metal [43]. AuNRs were synthesized at room temperature with $AgNO_3$ and $PdCl_2$ as metal precursors. By using acetone and acetonitrile as medium, AuNRs with 100–200 nm in width and few microns in length were produced.

Murthy and col. demonstrated the rapid one-step green synthesis of gold and silver NPs using fruit extract of *Averrhoa bilimbi Linn* [44]. The AuNPs with the average diameter about 50–150 nm and hexagonal or rhomboidal shape were synthesized. In general, AuNRs made by green sytheses are more unstable and their parameters are less controllable than those which are prepared by classical methods with CTAB.

Each other method varies form these three syntheses in concentration of the every single component and in additives. The control of AR and the yield are influenced by many factors as stability of the seed solution, concentration of surfactant or temperature.

4. Factors affecting gold nanorods synthesis

Nowadays, a big problem in the synthesis is the reproducibility of nanorod size, shape, and yield. The yield of rods provided by methods mentioned above was very low (~5%) in comparison with yield of NPs of another shapes. However, the yield could be improved by changing the reagent conditions like pH and purification methods [4]. The factors as aging time, variations in salt contcentration, solution temperature, solution pH or the sequence of mixing the seed and growth solutions can make differences in reproducibility [45]. The AuNRs length can be mainly influenced by surfactant properties for example Au ions and the surfactant micelles binding, Au ion in $[AuBr_4]^-$ instead of $[AuCl_4]^-$, formation of Au ions with larger micelles etc. [6,46].

4.1. Solution temperature

The morphology and AR of the AuNRs strongly depend on the reaction temperature. There are two different hypothesis explaining the dependence of the NRs length on solution temperature. The first one is reported by Perez-Juste [5]. He found out that the reduction in solution temperature leads to the formation of short NRs. On the other hand, Becker and col. revealed that in order to obtain the most homogeneous samples of AuNRs with high AR, the temperature should be held as low as possible [47]. This fact was also confirmed by Lee, who has reported that the increase of reaction temperature causes the decrease of NRs AR, but on the

other hand there is an increase in AuNRs width and the NPs are more uniform in size and shape [15].

4.2. Surfactant properties

Surfactant self-assemblies play an important role in the AuNRs preparation. Surfactant is necessary not only as an electrolyte but also for a AuNRs formation, solution stability etc. Formation of surfactant bilayer is one of the essential component in the anisotropic AuNRs growth. The stability is guaranted by noncovalent coating of NRs surface with a CTAB bilayer which prevents NRs aggregation. Length of surfactant tail influences the efficiency of AuNRs formation. It has been shown that shorter tail lengths cause the formation of AuNRs lower AR. CTAB contains long tail of 16carbons and bromide which initiates the rod growth. It is important to notice that CTAB bilayer is formed in a zipper-like mode (Figure 10) [40].

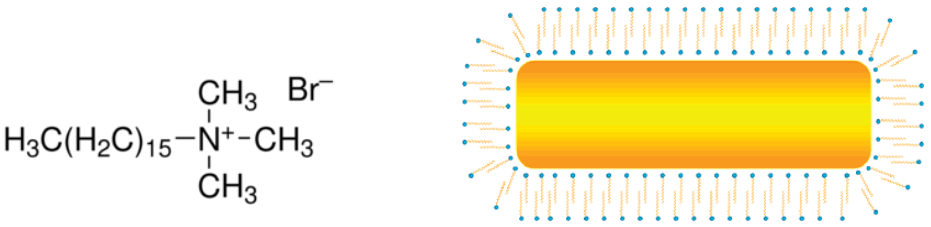

Figure 10 CTAB: detailed structure of CTAB (left) and AuNRs coated by a CTAB bilayer (right). Each CTAB molecule contains Br^- (blue spheres) and tail of 16carbons (yellow tail) [48]

The effect of CTAB concentration on the AuNRs formation and temperature during the synthesis are the most important milestones in their preparation [4]. Takenaka and col. have found out the dependence of CTAB concentration on NRs length. Their results show that NRs length grows with higher CTAB concentration. The NRs of high AR were obtained in the presence of high CTAB concentration during their growth in contrast to short NRs formation at the lowest tested CTAB concentration [24].As mentioned earlier, the temperature plays a key role during the AuNRs preparation. But still it is necessairy to respect the critical micelle temperature of surfactant during the synthesis. With increasing temperature, the surfactant solubility increases nonlinearly. It means that there is a certain temperature range in which the solubility is significantly increased. The temperature interval is called the critical micelle temperature (Krafft point ev. Krafft temperature). The Krafft point is the minimum temperature at which the surfactant molecules aggregate and form micelles in aqueous solution. The problem is that the aggregation could eventually results in the gelation of aqueous solution. The aggregation behavior is controled by several intermolecular forces, such as Van der Walls

interaction between hydrophobic chains, repulsive interaction between ionic head groups etc. but the true nature of the gelation stays unclear [49]. In conclusion, all syntheses in the presence of CTAB have to be parformed at the temperature higher than the Krafft temperature of CTAB (26 °C).

CTAB forms a double layer as already mentioned before. The alkylammonium groups ($-N(CH_3)_3^+$) of inner layer adsorb to the negatively charged AuNPs. The outer layer is directed outwards, towards the surrounding solvent and keeps the particles dispersed. CTAB molecules are strongly adsorbed mainly to the AuNRs long sides. The final complex of CTAB-stabilized AuNRs has a net with positive charge that is pH independent in aqueous solution [50]. If the CTAB concentration becomes too low, the double layer structure begins to disintegrate and new double layers are formed between two or more nanoparticles resulting in the aggregation (Figure 11) [47].

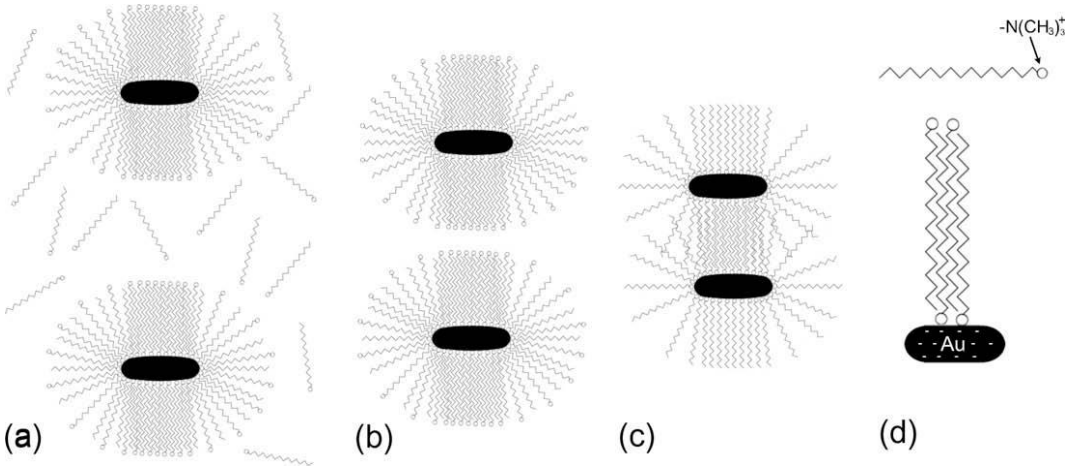

Figure 11 Illustration of CTAB concentration and stability of AuNRs in solution. (a) An excess of surfactant, (b) the double layers become unstable at lower concentrations; (c) and aggregate, (d) CTAB double layer attachtes to the negatively charged AuNPs

Korgel et al. reported that one of the significant factors in NR reproducibility is the supplier of the CTAB. They have proved that the sytheses using the same preparation protocol but CTAB from different suppliers resulted in different shape causing dramatic colour of NPs (Figure 12). The impurities in CTAB could be the reason of these different results [48].

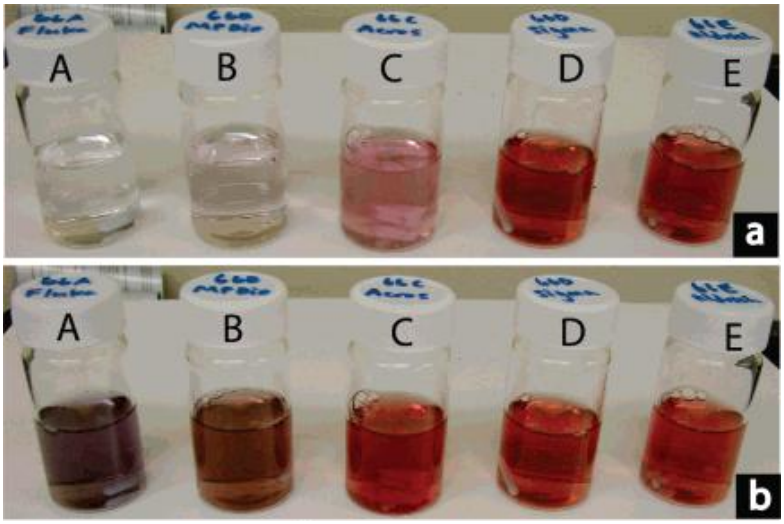

Figure 12: Au NPs prepared by the same procedure with CTAB from five different suppliers. The growth solutions after (a) 6 min and (b) 30 min [48]

There is another problem related to CTAB, namely free CTAB is known to be highly cytotoxic. In order to remain CTAB-rods soluble, it is necessary to remain concentration of free CTAB in solution above a certain value. Zubarev et al. reported a strategy to exchange of CTAB for its thiolated analogue (16-mercaptohexadecyl) trimethylammonium bromide (MTAB). The result was that the MTAB NRs have not only shown ~~a~~ highly increased stability to multiple purification compared to CTAB NRs, but they were also nontoxic [51].

Lee and col. found out that the power of reducing agent is influenced by changes in pH [15]. When the pH of solution is increased above 7, the reducing power is also increased and the AuNPs grow up before capping action of CTAB, which results in the formation of short NRs. When pH of solution is low (below 7), reduction rate is slower and NRs of high AR are synthesized using CTAB. Busbee has reported that in certain pH interval (pH = 2–6) AR of AuNRs could increase, but the notable growing in AR is accompanied by increasing polydispersity [52]. In conclusion, the control of pH could increase or decrease the NRs length, but also the polydispersity of final solution.

5. Modification and functionalization of gold nanorods

AuNRs modifications improve their efficiency and versatility. The possibility to modify their surface by various agents to obtain better chemical or physical properties is a big task, mainly to improve their solubility, stability and finally their biocampatibility for the purpose of their reliable medical applications (Figure 13).

Gold is known mainly for its strong affinity for hydrogen, and thus also for biologically important functional groups such as -SH, -NH_2 [10]. Therefore colloidal gold is also a good candidate as modification agent for futher functionalizations. The AuNPs can be used for example as a tool for improving sensing and luminescent properties. An application example is the porous silicon (pSi) modification by colloidal AuNPs to enhance the optical pSi response [53].

Toxicity of CTAB is one of the reasons why to modify AuNRs surface. AuNRs have been proved to display significant cytotoxicity to human cells because of the highly cytotoxic property of free CTAB [54]. But the AuNRs functionalization is very challenging mainly because of CTAB covering. If the CTAB structure around the rods is disturbed, complete or partial aggregation can happen easily during AuNRs functionalization. Consequently, it leads to lose the unique AuNRs optical properties [55].

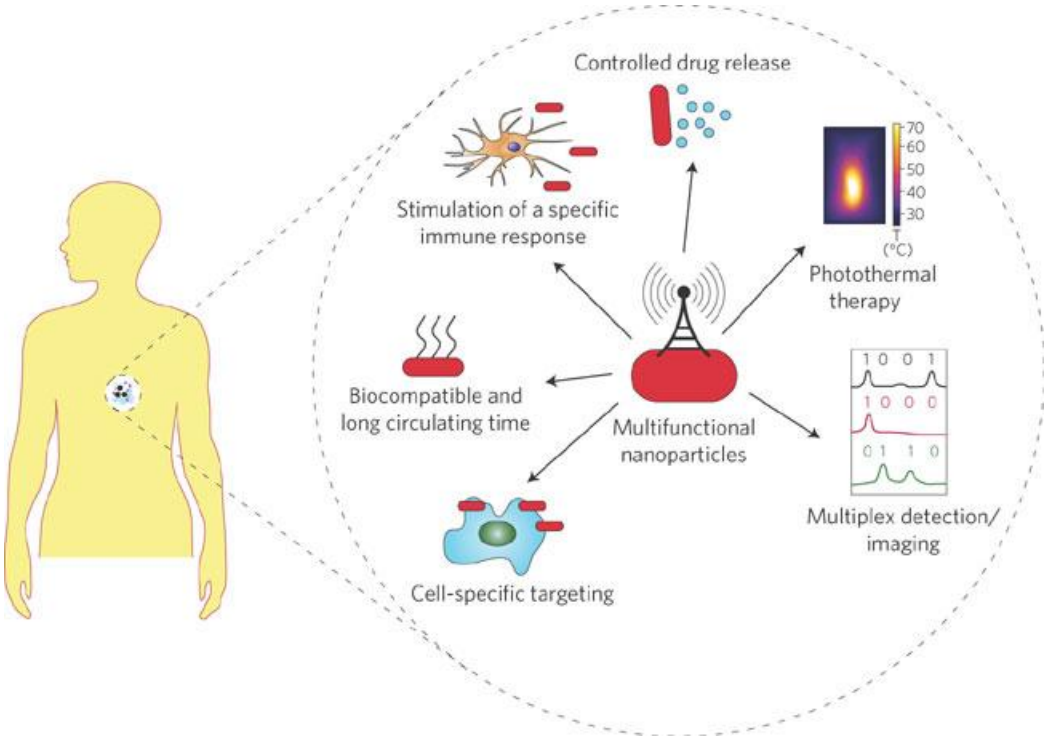

Figure 13 Requirements for ideal NRs used in biomedical applications [56]

Nowadays, glutathione tripeptide is used mainly for the purpose of eliminating the AuNRs toxicity. Wang and col. have modified AuNRs through robust Au–S bond formation by using zwitterionic oxidized glutathione [57]. Glutathione has proven to be an excellent ligand, usable for its coating because of its biostability, physiological pH and a large number of reactive groups.

A type of worm-like NRs has been synthesized by Chen and col. They have modified AuNRs with $Na_2S_2O_3$ or Na_2S to produce worm-like structures demonstrating higher sensitive property in LSPR than the original NRs. The longitudinal plasmon wavelength is limited only by properties of starting original. The approach is able to change AuNRs longitudinal plasmon wavelength selectively [58].

5.1. Modifications for photothermal therapy applications

Lately, many scientists started to prefere the AuNRs surface modification with silica. The main reasons are elimination of their cytotoxicity, improvement of their biocompatibility and the influence on extinction spectrum. Shen and col. reported that the longitudinal SPR band of AuNRs-SiO_2 is red shifted to about 30–840 nm upon the silica deposition [54]. Huang and col. have proved the increasing photothermal and radiation therapeutic effect as a result of using the synthesised folic acid-conjugated silica-modified AuNRs. The modified NPs also exhibited strong X-ray absorption for *in vivo* X-ray and computed tomography imaging (Figure 14) [59].

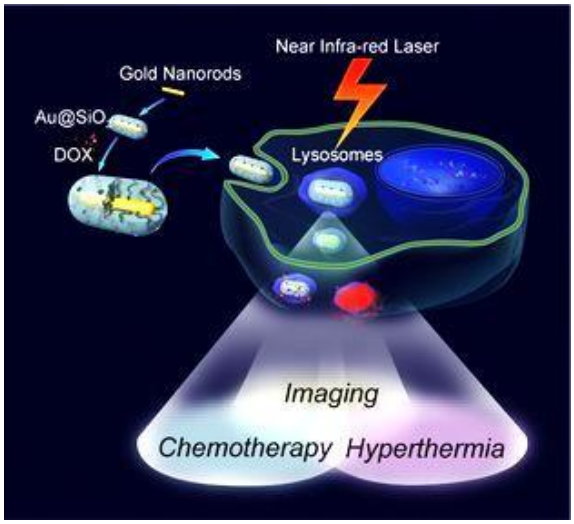

Figure 14 Silica-coated AuNRs and their biomedical applications: imaging, chemotherapy and hyperthermia. [60]

Futhermore, the silica-coated AuNRs can be additionally functionalized for targeted and noninvasive remote controlled drug delivery and photothermal therapy. DNA modification is one of the possibilities of capping and targeting agent (Figure 15) [61,62].

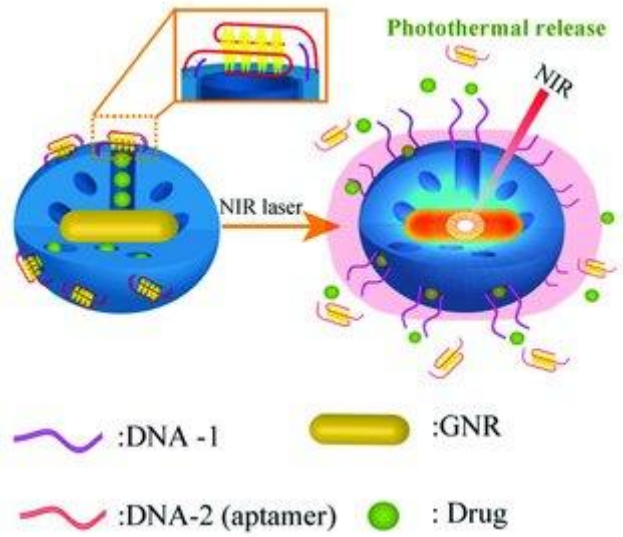

Figure 15 DNA-silica-coated AuNRs used for controlled drug delivery and photothermal therapy [61]

The next option how to reduce cytotoxicity and at the same time increase the photothermal effect is CTAB replacement by thiolated poly-ethylene-glycol (PEG) [63,64]. PEG modification also exhibit improvement *in vivo* stability [65]. Silica coated AuNRs could be conjugated with PEG in order to target the tumor precisely and increase the therapeutic efficacy [54]. The further functionalization can be also done by conjugation with CD33 antibody. Liopo and col. have reported that final product, CD33-PEG-AuNRs, has shown high level of accumulation for leukemia cell lines, and it was successfully used for nanothermolysis of human leukemia cells *in vitro* [66].

Poly-styrene-sulfonate (PSS) is also used, mainly for the replacement of CTAB from the NRs surface. The problem is that PSS-coated AuNRs show substantial cytotoxicity compared with PEG-AuNRs. PEG-AuNRs also exhibit better dispersion stability, in comparsion to the PSS-AuNRs which tend to aggregate and make clusters [67]. Gomez and col. have compared PSS-AuNRs with methyl-polyethyleneglycol-thiol (m-PEG-SH) coated AuNRs, mainly their stability and heating efficiency after irradiation with NIR light. Better results were obtained for m-PEG-SH-AuNRs, which were not only stable, but they also showed a potential as a biocompatible hyperthermic agent [68].

5.2. Interaction of gold nanorods with cells

Because of application in biomedicine, studies on the interaction between nanoparticles and cells have become increasingly important. There are a lot of factors which can influence the final interaction, such as cell type, AuNRs size, AuNRs surface modification or AuNRs surface charge.

Liu and col. investigated the surface and size effects of AuNRs on phagocytic and nonphagocytic cells [69]. They used two series of AuNPs with positively and negatively charged surfaces and sizes range of 16–58 nm. The results showed that the AuNRs with positive surface charge have higher cell internalization ability than those with negative surface charge in nonphagocytic HepG2 cells. In the case of phagocytic RAW 264.7 cells, the uptake extent of negatively charged AuNPs was similar with that of the positively charged AuNPs. The negatively charged AuNPs with a diameter similar to 40 nm have the highest uptake in both cells.

6. Characterization of gold nanorods

6.1. Cytotoxicity of gold nanoparticles

As was mentioned above, the AuNRs toxicity complicated their *in vivo* application. The MTT test is a tool for evaluating the cytotoxicity. NAD(P)H-dependent cellular oxidoreductase enzymes are capable of reducing the tetrazolium dye MTT-[3-(4,5-dimethylthiazol-2-yl)-2,5-diphenyl-tetrazolium bromide] to its insoluble form called formazan, which has a purple color. Viable cells with active metabolism convert MTT into a blue-purple colored formazan product with an absorbance maximum near 570 nm. This is the reason why the evaluation is done mostly by spectrophotometry at a wavelength of 570 nm. There is a rule that the higher absorbance caused by more intensive color in the hole, the higher percentage of living cells. Conversely, if the cells are dead, there is not any respiration at mitochondrial membrane, the blue formazan crystals do not form and the holes stay yellow [70].

The toxicity of non-modified and PEG modified AuNRs by MTT assay was investigated in several studies [54,62]. Lower systematic toxicities of AuNRs were proven in the case of modified AuNRs in comparsion with non-modified AuNRs. The cell viability remained above 95% when the cells were incubated with modified AuNRs at the different concentrations. In

contrast, the non-modified AuNRs showed increased toxicity (above 35% dead cells) caused by CTAB (Figure 16).

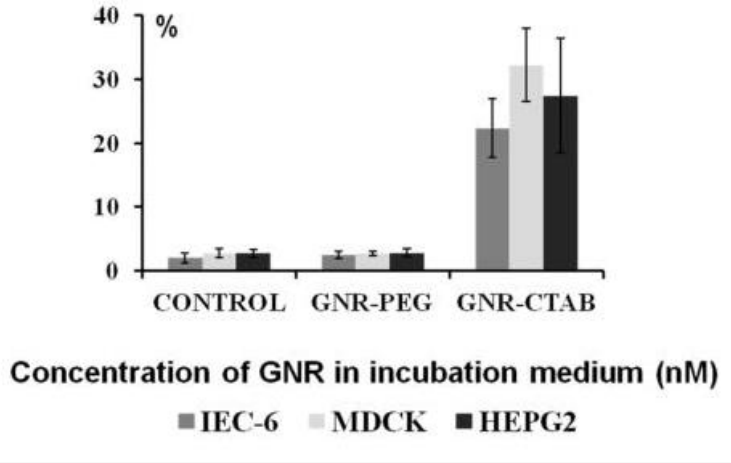

Figure 16 Dose dependence effects of AuNRs on IEC-6, MDCK and HEPG2 cell lines: percentage of dead cells after incubation with GNR coated with CTAB or PEG [62]

Studies also included a photothermal effect on cell viability [54]. It was reported that the direct irradiation of the cells showed a big effect on cell viability - about 64% of cells were killed by modified AuNRs combined with NIR laser.

6.2. Scanning Electron Microscope

Scanning electron microscope (SEM) is one of methods for the physical surface nanostructure analysis with 2 million as a maximum level of magnification [71]. This type of analysis allows to gain a lot of knowledge about sample physical properties, namely its structure, optical properties, conductivity, etc. SEM is a device used for visual surface analysis. Moving narrow beam of electrons is utilized for imaging of surface. The beam interacts with the atoms forming the sample surface to give a signal. Two types of signals are produced by SEM - secondary electrons (SE), back-scattered electrons (BSE). The SE signals result from interactions of the electron beam with atoms at or near the sample surface. The BSE are reflected from the sample by elastic scattering, so the BSE images can provide information about the distribution of different elements in the sample. The signal varies according to the surface character. The final three-dimensional image showing the surface structure is made by the accumulation of scattered electrons signals.

6.3. Transmission electron microscopy

Transmission electron microscopy (TEM) is a microscopy technique allowing observation beyond the surface of specimen to a thickness of 100 nm at high magnification and high resolution (50 million magnification level) [72].

The basic principle is the same as the light microscope but the electrons are used instead of light. Electromagnetic lenses focus the electrons into a very thin beam, which travels through the sample. Some of the electrons are scattered and disappear in dependence on the material density. The two-dimensional image is arisen from an interaction of unscattered electrons and a fluorescent screen at the microscope bottom. Different parts are displayed in varied darkness according to their density.

TEM analysis shows more detailed information about nanometer sized structure than SEM. That is why majority of AuNRs characterizations are done by TEM observation [5,64,67].

6.4. Dynamic light scattering and Zeta potential

Dynamic light scattering (DLS) is nondestructive optical method, used for the characterization of colloidal particles by determining the diffusivity of solid particles in a liquid medium. DLS is based on measurements of light intensity fluctuations that is scattered by moving particles. The particles move on the basis of Brownian motion. If there are not any measured particles or there is not any movement in the sample, the amount of scattered light is null or constant [73].

The sample is irradiated by monochromatic coherent light beam during the measurement. The fluctuation dynamics in scattered light intensity is monitored. The faster movement of particles in the system is, the faster changes in the intensity of scattered light is. Particle size is measured on the principle that smaller particle is moving in the system faster than large one. Diffusion coefficient is then determined based on the correlation analysis. DLS results give intensity distribution, volume distribution, and number distribution of AuNRs [74].

Zeta potential is a term for electrokinetic potential in colloidal systems. It is the potential difference between the stationary layers of fluid attached to nanoparticles (in this case AuNRs) and the dispersion medium. A value of +/- 25 mV can be taken as the arbitrary value that separates low-charged surfaces from highly charged surfaces. The value indicates the stability of colloidal dispersions. For very small particles, high zeta potential (negative or positive) means

good stability, while colloid solution with low zeta potentials tend to be unstable and aggregate [75,76].

Liopo has used this method to find out changes of AuNRs surface charge after modification. After the modification, zeta potential changed from strong positive charge for CTAB-AuNRs to slightly negative charge for C_{33}-PEG-AuNRs (Figure 17) [64,65].

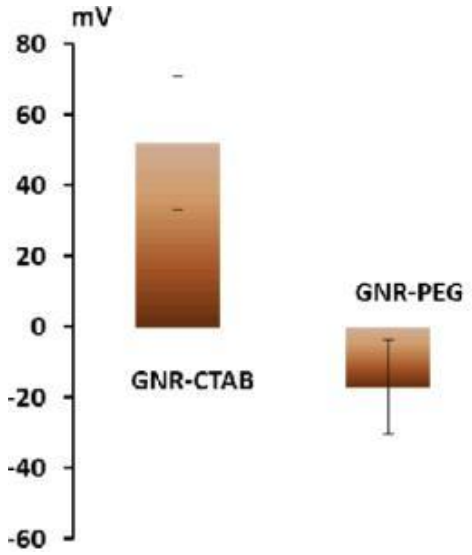

Figure 17 Zeta-potential for AuNRs with different surface ligands (CTAB and PEG) [66]

6.5. Spectrofluorometer

Spectrofluorometer is a device using the interaction of electromagnetic radiation with the sample for characterization of the optical properties (absorption and emission). The radiation passes through the excitation monochromator and falls onto the sample in the form of the excitation beam. Emitted fluorescent radiation measured in the direction perpendicular to this excitation beam first passes through the emission monochromator and then is detected with a photomultiplier. The sensitivity and spectral resolution of the measurement has been given by setting a wavelength and a width of monochromators slits. The result of the analysis is the spectrum showing the dependence of emitting energy or the excitation radiation on wavelength.

AuNRs spectra are usually mesured in UV-VIS region. Multiple plasmon bands are formed by AuNRs. In general, one peak is formed for the transverse plasmon and one peak for the longitudinal plasmon (see chapter Plasmon resonance of gold nanorods) [5,65].

6.6. Fourier transform infrared spectroscopy

Fourier transform infrared spectroscopy (FTIR) is a technique which works in infrared part of spectrum. The spectral data are collected in a wide spectral range in the same time. This technique means a significant advantage over dispersive spectrometers which measure intensity over a narrow range of wavelengths in time.Using a simple FTIR spectroscopic method, it is possible to quantitatively determine the the AuNRs surface structure, for example CTAB that is replaced by the functionalizing agent [41,63].

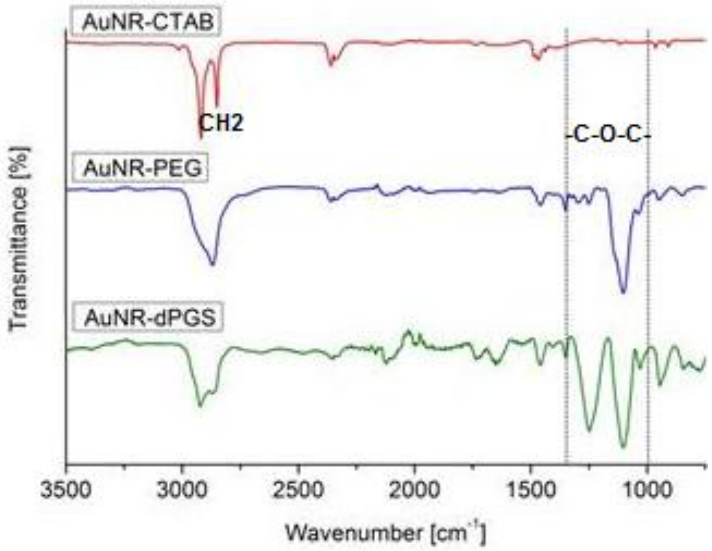

Figure 18 FTIR spectra for CTAB-AuNRs and PEG-AuNRs [77]

6.7. Energy dispersive X-ray spectroscopy

Information about the chemical properties of sample is obtained by the energy dispersive X-ray spectroscopy (EDX). The technique is used to analyze the elemental composition of the sample. Specific area on the surface can be targeted precisely with imaging capabilities of SEM or TEM, which EDX may be part of. The basic EDX principle works on unique atomic structure element which allow unique set of peaks on its X-ray spectrum.

The emission of characteristic X-rays is stimulated from a specimen by a high-energy beam of charged particles such as a beam of X-rays, that are focused into the sample. The emitted X-rays are a result of the de-excitation of core electron holes created by the high energy electron beam. The X-rays number and energy emitted from a specimen are measured by an energy-dispersive spectrometer. The result is the spectrum showing the peaks corresponding to the various elements of real representation.

7. Experimental part

7.1. Materials

Name	Formula	Information	Provider	CAS No.
Chloroauric acid	$HAuCl_4.3H_2O$	≥49.0%, granular	Sigma Aldrich	16961-25-4
Cetyltrimethylammonium bromide (CTAB)	$C_{19}H_{42}BrN$	ultra, ≥99.0%, crystalline	Fluka	57-09-0
Sodium borohydride	$NaBH_4$	≥98.5%, granular	Sigma Aldrich	16940-66-2
Silver nitrate	$AgNO_3$	≥99.5%, crystalline	Sigma Aldrich	7761-88-8
L-Ascorbic acid	$C_6H_8O_6$	BioXtra, ≥99.0%, crystalline	Sigma Aldrich	50-81-7
Polyethylenglycole (PEG)	$C_{2n}+2H_{4n+6}O_{n+2}$	average Mn 4,000	Aldrich	81240
Tetraethylorthosilicate (TEOS)	$SiC_8H_{20}O_4$	98 %	Sigma Aldrich	78-10-4
Methylthiazoletetrazolium bromide (MTT)	$C_{18}H_{16}BrN_5S$	98%	Sigma Aldrich	298-93-1
Sodium dodecyl sulfate (SDS)	$CH_3(CH_2)_{11}OSO_3Na$	99%	Sigma Aldrich	151-21-3

Deionized water (Millipore, with Millipore Quantum EX Ultrapure Organex Filter Cartridge) was used in all the preparations.

7.2. Equipment and characterization tools

The fundamental size and shape analysis was done with Scanning electron microscope (SEM) Tescan FE MIRA II LMU by Marian Marik. The NPs element analysis was performed using EDX detector. Namely, SEM Tescan is equipped with an element detector system based on energy dispersive analysis using EDX X-Max 50 purchased from Oxford Instruments. The informations about shape and size was obtained from analytical transmission electron

microscope Jeol, JEM 2100F, 200kV, with Schottky autoemission cathode, from Institute of Physics of Materials at Academy of Sciences in Brno. The high-resolution images were evaluated by using software Gatan, DigitalMicrograph by Mrs. Naděžda Pizúrová. Before the SEM and TEM observation, 1 mL of each final solution was centrifuged for 30 min at a speed of 14.000 rpm to separate the particles. The supernatant was removed after the centrifugation and the residue was redispersed in 1mL of ultra-pure water and centrifuged again. After repeating the above procedures for several times, the final precipitate was redispersed in a 1 mL of ultra-pure water based on the uantity of precipitate. For SEM observation, 5 μL of the AuNRs were dropped on the silicon wafer (coated with Al, Ni or Ti thin layer) and dried in the air.

To analyse the optical properties of AuNPs, UV-VIS absorbance spectra of samples were measured by using the Spectronic Helios Alfa spectrophotometer from Faculty of Chemistry, BUT. UV-VIS measurements were performed for wavelengths ranging from 300 nm up to 1100 nm using 4 mL of sample solution in a spectrophotometer cuvette (Sigma Aldrich).

Zeta potencial, AuNPs size and their quantity were tested by DLS detector Zetasizer Nano purchased from Malvern Instruments by Michal Kalina at Faculty of Chemistry, BUT. The volume distribution was obtained from intensity distribution based on the tabulated values of refractive material index, in this case gold. 3 mL of each sample was measured in a disposable cuvette. For Zeta potential, samples were analysed using a standard zeta cuvette. The samples were analysed three times at 25 °C.

Infrared spectra were measured using FT-IR Spectrometr Thermo Scientific Nicolet iS10 by Vojtěch Enev at Faculty of Chemistry, BUT. All spectra were recorded at the resolution of 4 cm^{-1} over the wave number range of 400–4000 cm^{-1}. Before the FT-IR analysis, 20 mL of sample was centrifuged and freeze-dried in a freeze dryer Bench Top K. Samples were freeze-dried in a lyophilizer condenser at -105 °C for 24 h. After that the samples were lyophilized in condenser at temperature of -105 °C and pressure of 1 microbars. The lyophilization time was 12 h.

MTT assay was performed on Human Embryonic Kidney 293 cells (HEK 293). HEK cells were plated into 96-well plates at a density of $2–4 \cdot 10^4$ cells in 100 μL of culture medium Eagle's Minimum Essential Medium (EMEM). After 24 h of incubation, the medium was replaced with 100 μL of AuNRs suspension of variable concentrations (50, 100, and 200 μg/mL) prepared in deionized water. Three replicate wells were employed for each tested AuNRs concentration. Negative controls were made by cells which were not exposed to AuNRs.

The medium was removed from wells by micropipette. Next, 30 µL of solution containing 3 mg/mL of MTT dissolved in deionized water was added to each well after 24 h of AuNRs exposure. Blue-purple colored formazan product was expected to be formed by MTT after 3 h of incubation at 37 °C. At this point, the medium was removed and the formazan was dissolved in 100 µL of 10% sodium dodecyl sulfate and kept in dark and cold place during the night. After 1 day, a resulting violet solution with absorbance at 560 nm was measured by microplate reader Infinite M200 Pro, Tecan at Mendel University. The cell viability percentage was expressed by the equation:

$$RGR = \left(\frac{A_{sample}}{A_{control}}\right) * 100, \quad (1.1)$$

$$A_{sample} = \frac{(A_1+A_2+A_3)}{3}, \quad (1.2)$$

where A_{sample} is the absorbance average of three measured samples (A_1, A_2, A_3) at one concentration and A_{control} is the negative control of absorbance [78].

7.3. Preparation and modification of gold nanorods

AuNRs were synthesized by using modified seeding method with CTAB as a surfactant [46]. The first step before each synthesis was to prepare CTAB in aqueous solution and heated it to at least 26 °C (Krafft point of CTAB) in warm water bath until the CTAB was well dissolved. Everytime, it was also necessary to make a fresh $NaBH_4$ solution and cool it to a temperature of 5 °C. These steps make the AuNRs preparation faster, more efficient and successful.

7.3.1. Preparation of gold seed solution

Seed solution contained 5.0 mL of 0.2 M CTAB aqueous solution mixed with 5.0 mL of 0.0005 M $HAuCl_4$. Then, 0.6 mL of freshly prepared ice-cold (t ≈ 5 °C) 0.01 M $NaBH_4$ was added under vigorous stirring. The colour immediatly changed to yellow-brown, which indicated the formation of small anisotropic AuNPs (≈ 1 nm). After the solution was stirred for next 2 min and then it was gently heated (≈ 30 °C) for at least 25 min to well decompose all $NaBH_4$. The seed solution was usually used immediately after its preparation, at the latest within 24 hours. The schematic illustration of preparation can be seen in Figure 19.

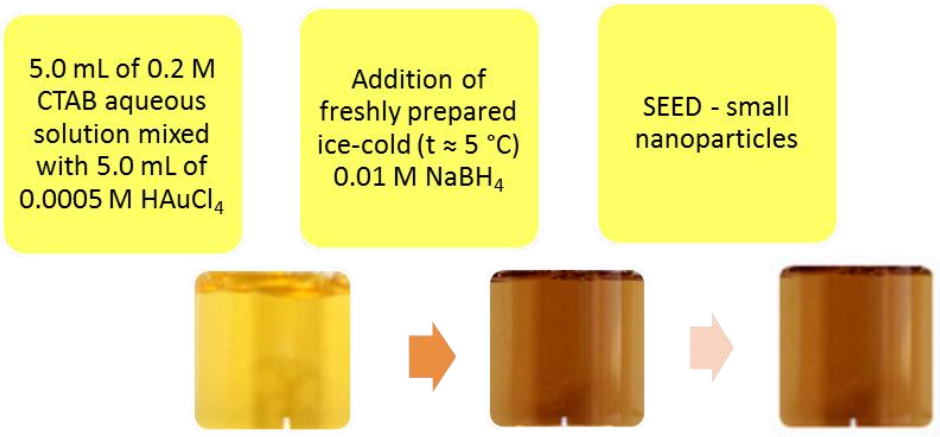

Figure 19 Synthesis scheme for seed solution

7.3.2. Preparation of growth solution

Growth solution was made by mixing of 5 mL of 0.2 M CTAB with 5 mL of 0.01-0.001 M $HAuCl_4$. The solution turns opalescent yellow. After gentle stirring, 0.5–2 mL of 0.08 M ascorbic acid was added and it was shaken. Ascorbic acid as a mild reducing agent changed the growth solution from yellow to colorless indicating the reduction of gold (III) to gold (I). Finally, 0.15–0.45 mL of 0.004 M $AgNO_3$ at 25 °C was added. The protocol of preparation is demonstrated by the scheme in Figure 20.

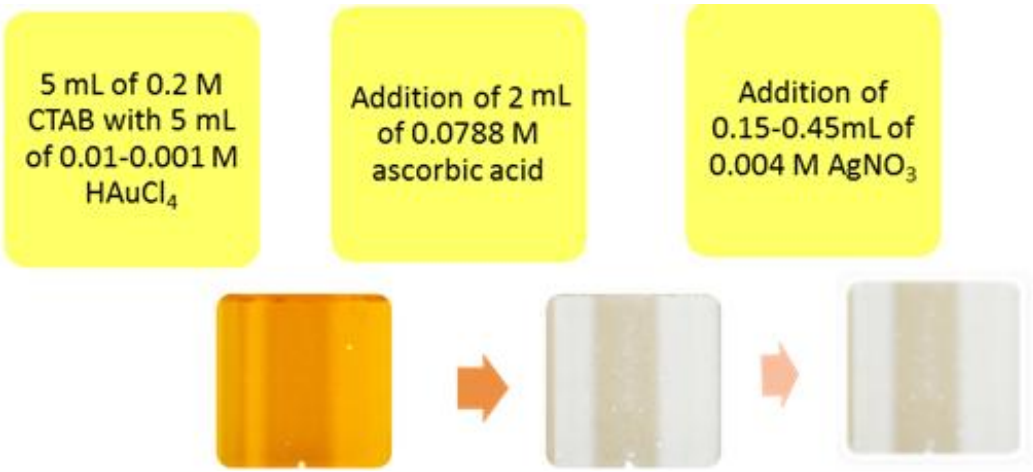

Figure 20 Synthetic scheme for growth solution

The final AuNRs were formed by the addition of 50−160 µL of the seed solution to the growth solution at 27–30 °C. The color of the solution gradually changed to dark blue during 5 min. Similarly, the scheme of synthesis is illustrated in Figure 21.

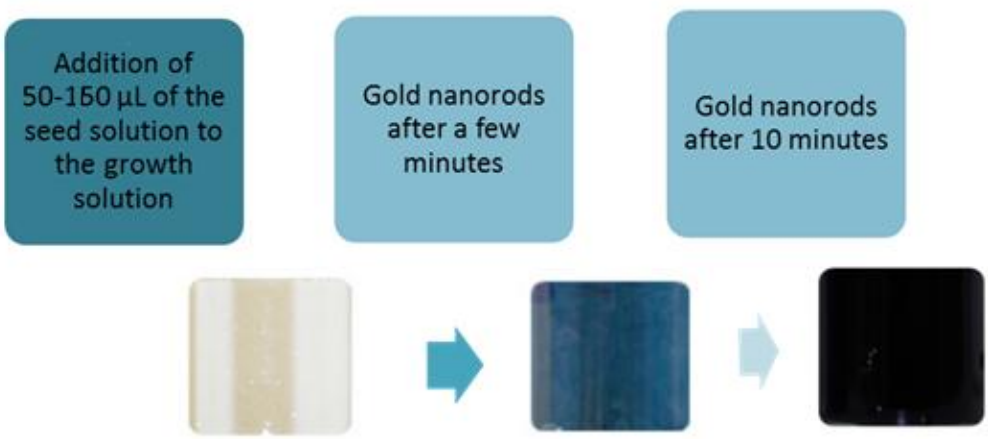

Figure 21 Synthetic scheme for gold nanorods

Individual syntheses differed in growth solutions, specifically in various $HAuCl_4$ and $AgNO_3$ concentrations and various amounts of added seed solution (Table 1).

Table 1 Preparation conditions of individual samples

Sample	c[$HAuCl_4.3H_2O$] in growth / M	Seed / µL	$AgNO_3$ / µL
1.	0.01	120	250
2.	0.005	120	250
3.	0.001	50	250
4.	0.001	80	250
5.	0.001	120	250
6.	0.001	160	250
7.	0.001	50	150
8.	0.001	50	350
9.	0.001	50	450

8. Results and discussion

The sedless silver-assisted AuNRs growth was used for the AuNRs preparation. The method is based on combining seed solution containing gold spherical nanoparticles (AuNSs) with a growth solution containing gold salt (chloroaurate), surfactant (CTAB), reducing agent (ascorbic acid) and small amount of silver.

The influence of the concentration of $HAuCl_4$ and $AgNO_3$ in growth solution and the amount of added seed on the final product was investigated. The synthesis conditions of AuNRs were modified in order to prepare AuNRs with different length, width, AR, and consequently the optical properties. Whatever conditions were used, the stability was the same in every case. From the macroscopic point of view, the colloidal solutions of AuNRs were relatively stable at the room temperature. The stability was probably ensured by noncovalent coating of NRs surface with a CTAB bilayer which prevented aggregation.

The formation of AuNRs was primarily investigated by using UV-VIS spectroscopy. Consequently SEM, DLS and Zeta potential analyses were used for AuNRs characterization. The additional AuNRs modification with PEG was investigated by FTIR analysis. In the end, the cytotoxicity of final product by MTT test was examined.

8.1. UV-VIS reagents characterization

The UV-VIS analysis was chosen as one of the basic AuNRs characterization due to the multiple absorption bands, namely the first formed for the transverse plasmon and the second one for the longitudinal plasmon. The typical spectrum profile could be recognized very easily. Moreover, the knowledge about the position of absorption maximum is very important AuNRs feature required for further applications. These are the main reasons which make the UV-VIS analysis very fast, simple and useful characterization tool.

UV-VIS spectra of simple reagents were measured in order to observe if the final AuNRs spectra are not distorted (Figure 22). The spectroscopic analysis showed that all the reagents have their absorption maximum at 300 nm. Building on this information, it can be said that the potential distortion influencing the final AuNRs spectra would be right at the beginning of UV-VIS region.

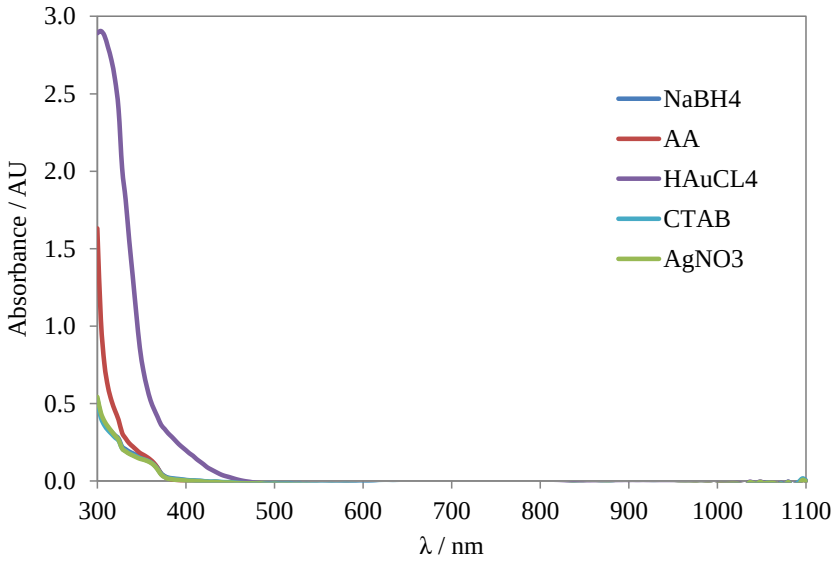

Figure 22 UV-VIS absorbtion spectra of reagents used in AuNRs synthesis: c[$NaBH_4$] = 0.01 M, c[AA] = 0.08 M, c[$AgNO_3$] = 0.004 M and c[$HAuCl_4$] = 0.01 M, c[CTAB] = 2 M

The final ARs of NPs are not influenced by the growth solution as much as by the seed solution. The UV-VIS spectra of growth solution of different age were measured to investigate how the time influences the resulting optical properties (Figure 23). It was found out that the growth solution absorbance increased with the time and showed a maximum at 800 nm. The problem was that the NPs contained in growth solution were very unstable and the solution degraded in 5 h.

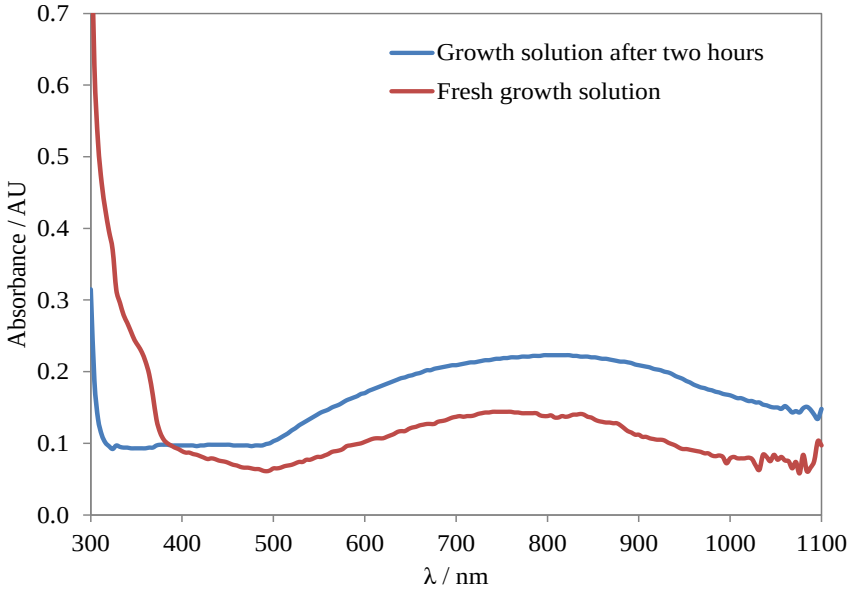

Figure 23 UV-VIS spectra of growth solutions of different age (right after the preparation and after 2 h of aging)

8.2. CTAB characterization

CTAB was used as a surfactant in all synthesis. Usage of CTAB made AuNRs preparation complicated because of its poor solubility. Thus, the first step before each synthesis was to well dissolve CTAB. The CTAB needed to be heated gently in warm water bath under stirring for achieving a pure solution before its application (Figure 24**Chyba! Nenalezen zdroj odkazů.**). It was necessary to respect the critical micelle temperature of CTAB during the synthesis, therefore the solution had to be heated up to 26 °C. If the temperature increased too vigorously or the stirring was not continious, the aqueous solution turned into gel solution.

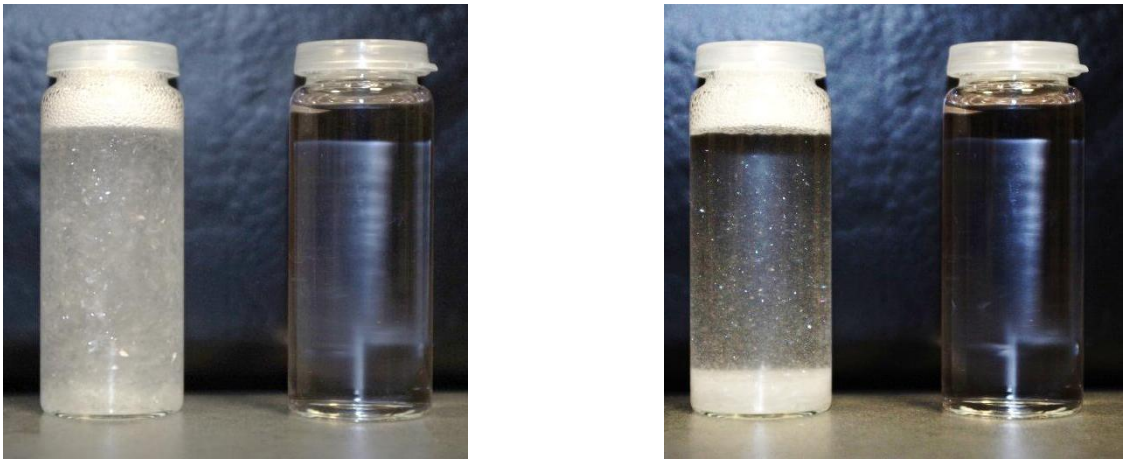

Figure 24: Photos of two CTAB samples being heated up (right) and not being heated up (left), after 5 min (left photo) and after one hour (right photo)

A big problem was also the impossibility of complete CTAB removal from colloid nanoparticles. Small AuNPs were not visible under a layer of organics originated from CTAB in SEM micrographs (Figure 25). Although all final solutions were centrifuged several times to precipitate the particles, remnants of CTAB always remained in the sample. This made the AuNPs analysis significantly more difficult and challenging.

Figure 25 SEM image of organic layer from seed solution with 100 µm CTAB crystals (bright slices)

It was also very difficult to differentiate between the CTAB crystals (Figure 26) and AuNPs during the SEM analysis by naked eye. Therefore, it was necessary to use EDX analysis for element (qualitative) characterization (Figure 27). According to the results of EDX analysis of CTAB, the entire surface was covered by organic layer (which was proved by the presence of Br and O) – in this case the surfactant corresponded to CTAB residues and by elements that the carrier medium contained – i.e. nickel (Ni), aluminium (Al), and silicon (Si).

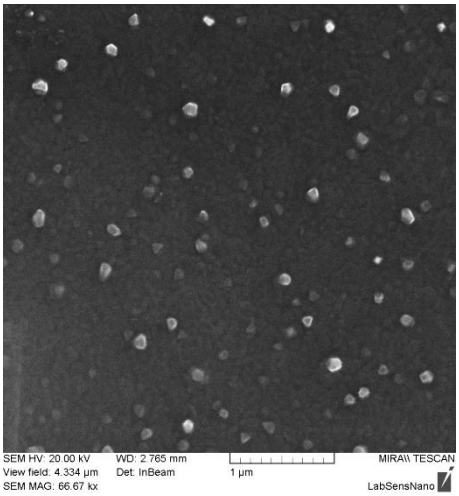

Figure 26: SEM characterization of pure CTAB (bright stains of 200 nm) on Ti substrate

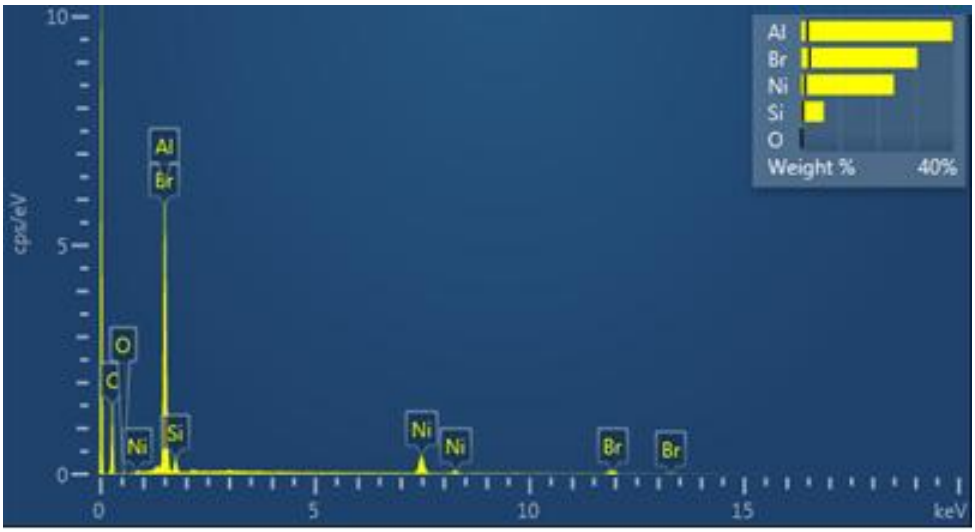

Figure 27: Elemental composition of the CTAB sample on Ni-Si substrate

8.3. Seed characterization

The seed solution preparation is the first step in AuNRs synthesis. The Au seed size and added amount of seed solution into metal salt is crucial for varying the final product size.

The expected particles size was around 3.5 nm (according to original work). DLS analysis proved that AuNPs of 1 nm, 50 nm and 500 nm were synthesized (Figure 28). Based on the SEM analysis it is estimated that bigger nanoparticles (50 nm and 500 nm) corresponded to CTAB crystals and clusters (Figure 26). From the volume distribution, it can be seen that the particles of around 8 nm in diameter were the most represented (Figure 29). It indicates that seed solution was highly monodispersed, with an average size of 1–10 nm.

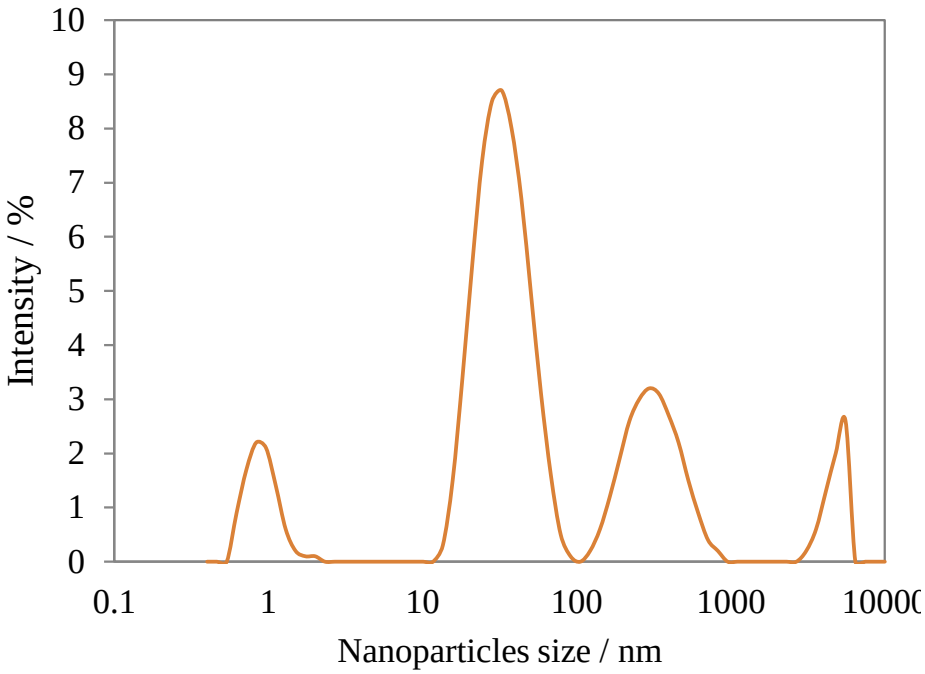

Figure 28 DLS analysis of seed solution: size distribution

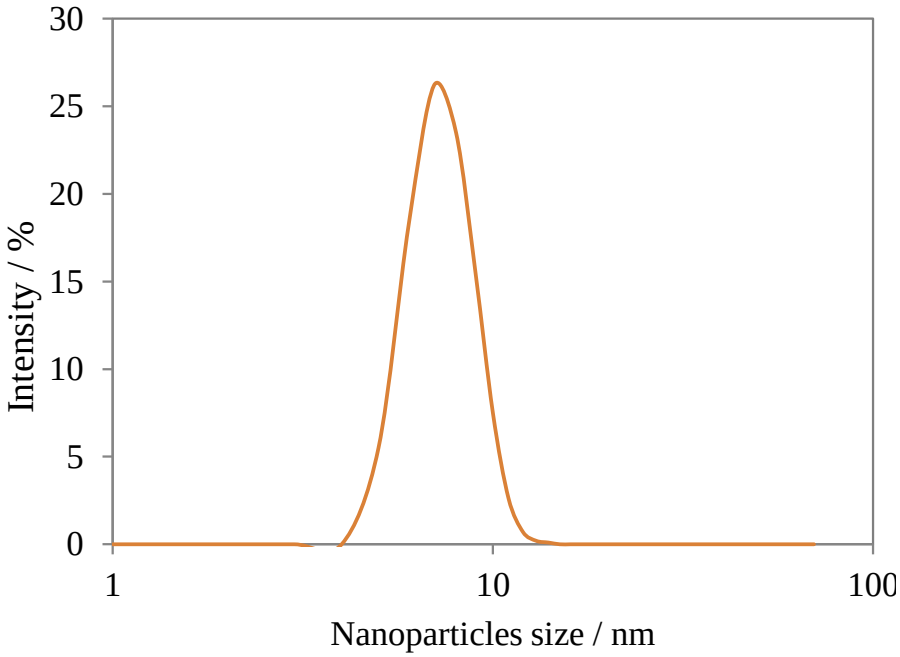

Figure 29 DLS analysis of seed solution: volume distribution

The seed solution was also characterized by zeta potential measurement. The analysis confirmed the expectation that the solution would have a positive zeta potential due to the presence of quarternary ammonium on CTAB [76]. Consistent shift to a positive zeta potential value around 57.5 mV was showed by this analysis. This value also indicates that the solution was highly stable. pH of seed solution was 4.27 at 25 °C. Very important results were

demonstrated by UV-VIS analysis (Figure 30). The fresh seed solution spectrum exhibits decreasing character with no peaks over the measured wavelenght range (300–1100 nm) which is typical result for every seed solution [21]. But two weeks old seed solution presented one significant peak in its absorption spectrum at 550 nm, which is typical for nanospheres (NSs). It could indicate the Ostwald ripening has happened which increases the sizes of AuNPs and forms NSs [79].

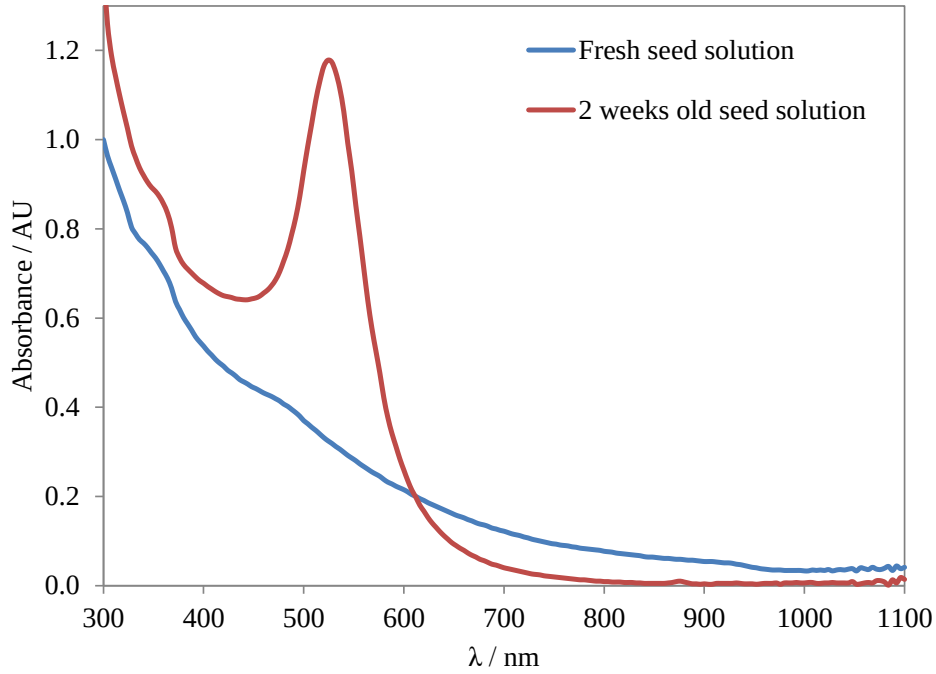

Figure 30 UV-VIS spectra of seed solution formed with c[$HAuCl_4.3H_2O$] = 0.0005 M: fresh solution: 1 nm AuNPs, 2 weeks old seed solution: 20 nm AuNSs

SEM characterization of seed solution was not possible because of remnants of organic compounds in the form of CTAB, which were presented even after several centrifugation (Figure 25) and thus covered the proper Au seeds. This is the main reason why TEM characterization was necessary. TEM analysis confirmed the results from DLS analysis. The fresh solution contained NPs mostly around 2–10 nm (Figure 31), but also NPs around 40 nm (Figure 32). It was also found out, that the solution became unstable and aggregated into bigger clasters after a few hours due to Ostwald ripening (Figure 32).

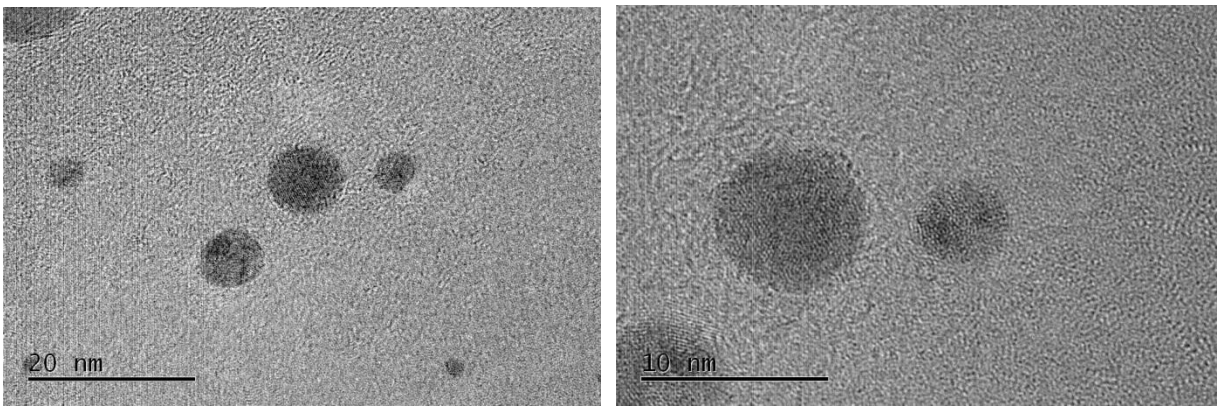

Figure 31 TEM characterization of fresh seed solution: AuNSs with diameters 2–10 nm, scale bars: 20 nm (left) and 10 nm (right)

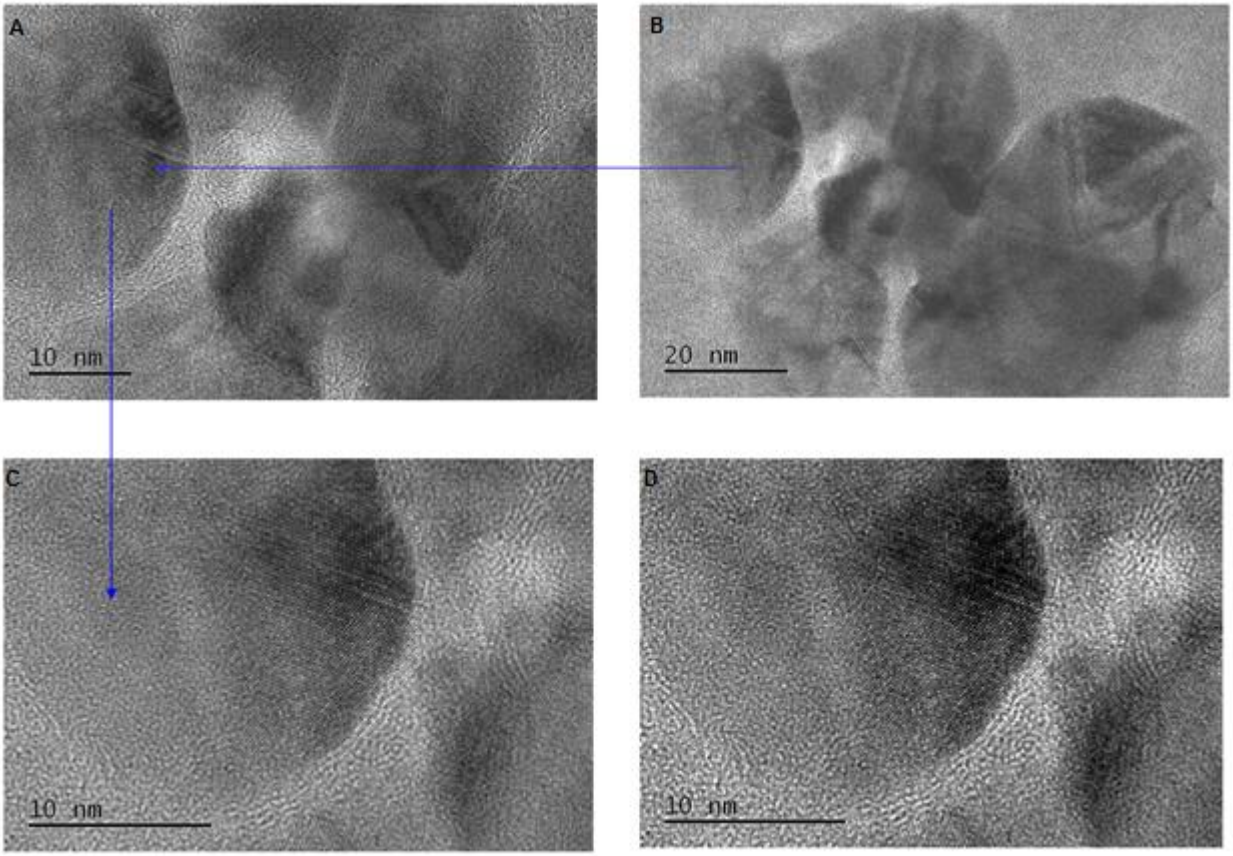

Figure 32 TEM characterization of seed solution after a few hours. Detailed images of AuNPs with diameters 10–30 nm (A, C, D) and the original (B), scale bars: 10 nm and 20 nm

8.4. AuNRs characterization

8.4.1. Influence of amount of added seed solution

As already mentioned, the size of NPs contained in seed solution and the amount of added seed solution to a growth solution play one of the decisive roles for AR of AuNRs. The influence of added amount of seed having the constant size was examined using four different samples (Table 2). The amount was varied from 50 μL to 160 μL. AuNRs with the highest AR were prepared with 50 μL of added seed solution (Figure 34). The higher seed amount was added into a growth solution, the lower AR of AuNRs was formed. This conclusion is supported by the opinions in already published articles [4,5].

Table 2 Evaluation of samples with different amount of seed solution added to growth solutions

Sample	c[$HAuCl_4.3H_2O$]/M	Seed/μL	c[$AgNO_3$]/M	Width/nm	Length/nm	AR	λ_{max}/nm
3	0.001	50	250	18	35	1.9	632
4	0.001	80	250	25	35	1.4	624
5	0.001	120	250	20	32	1.6	632
6	0.001	160	250	15	20	1.3	616

The LPSR is closely related to AuNRs size. The assumption was that the position of maximum absorbance would increase with increasing AR. UV-VIS spectra showed the highest LPRS at 632 nm for the sample with the lowest added seed amount (Figure 33) thereby confirming the expectation. The spectra also showed a big response right at the spectra beginning. this response is probably caused by oversaturation of growth solution by ascorbic acid, which can be proved by low pH of solution (2.57).

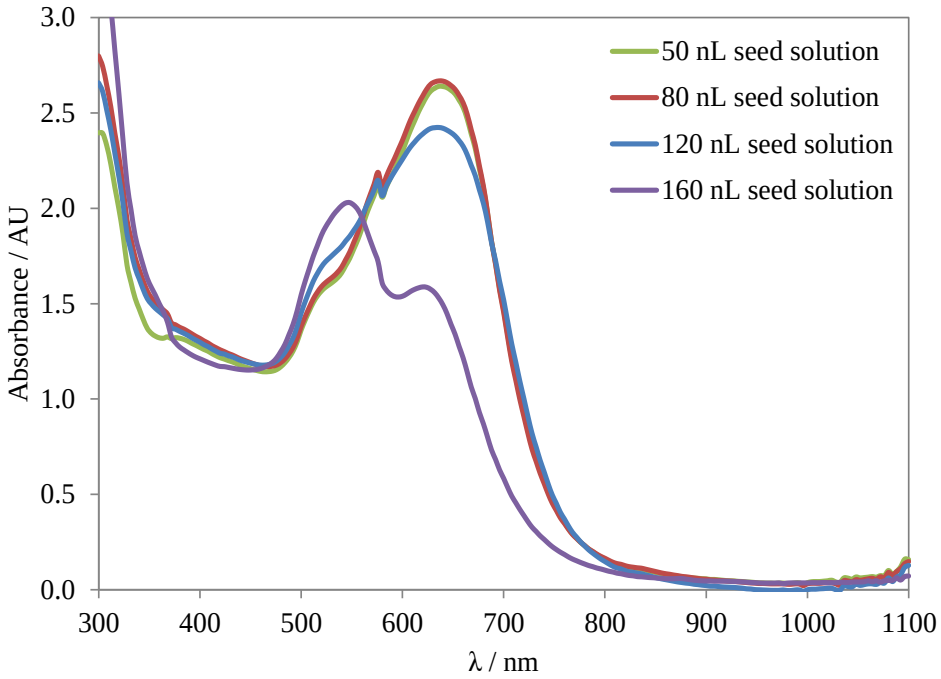

Figure 33 UV-VIS spectra of AuNRs formed with different amount of added seed solution

SEM analysis visualized the AuNRs properties as size, distribution, uniformity, etc. SEM images showed the presence of AuNRs in different concentrations depending on the amount of added seed. The highest concentration of AuNRs with lenght of 32 nm was gained in the sample 5 prepared with 120 µL of seed solution (Figure 36). In this case, SEM evaluation revealed the monodisperse NRs uniformly distributed on the substrate. The robustest NRs, but in very low concentration, were prepared with 80 µL of added seed (Figure 35). The tic-tac like NRs with the shape very similar to nanocubes have the resulting AR almost equal to 1. The worst result regarding the quality and quantity was obtained by adding the biggest volume of seed solution (160 µL) into a growth solution (Figure 37). The resulting product contained mainly the NSs, with low uniformity and distribution on the substrate. The NRs were formed in very low yield relative to the NSs.

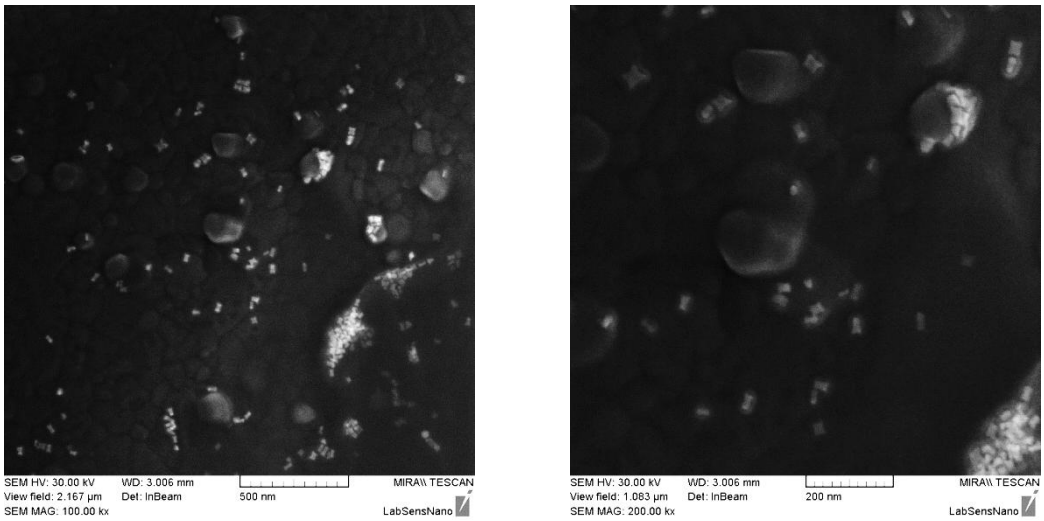

Figure 34 SEM images of sample 3: gold nanorods at magnification of 100 nm (left) and 200 nm (right)

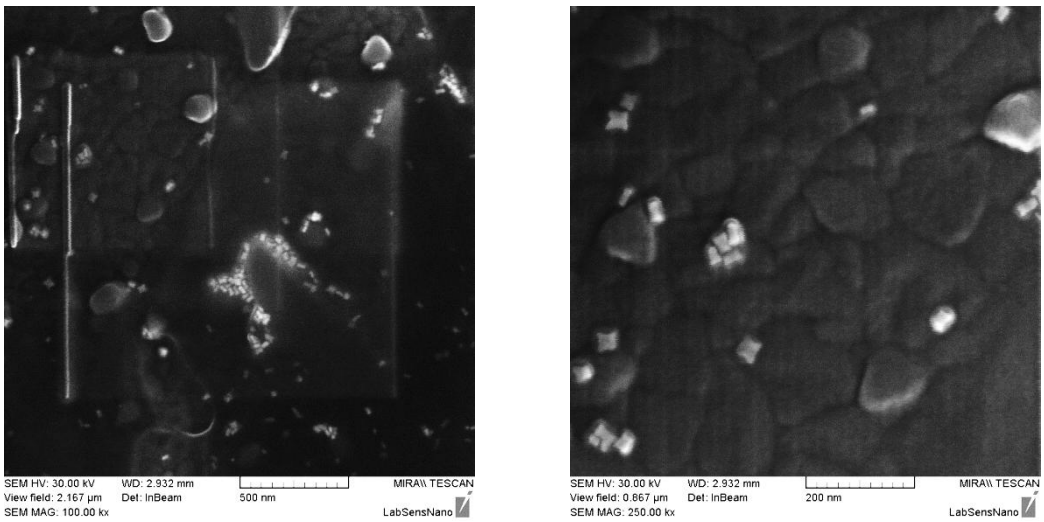

Figure 35 SEM images of sample 4: gold nanorods at magnification 100 nm (left) and 250 nm (right)

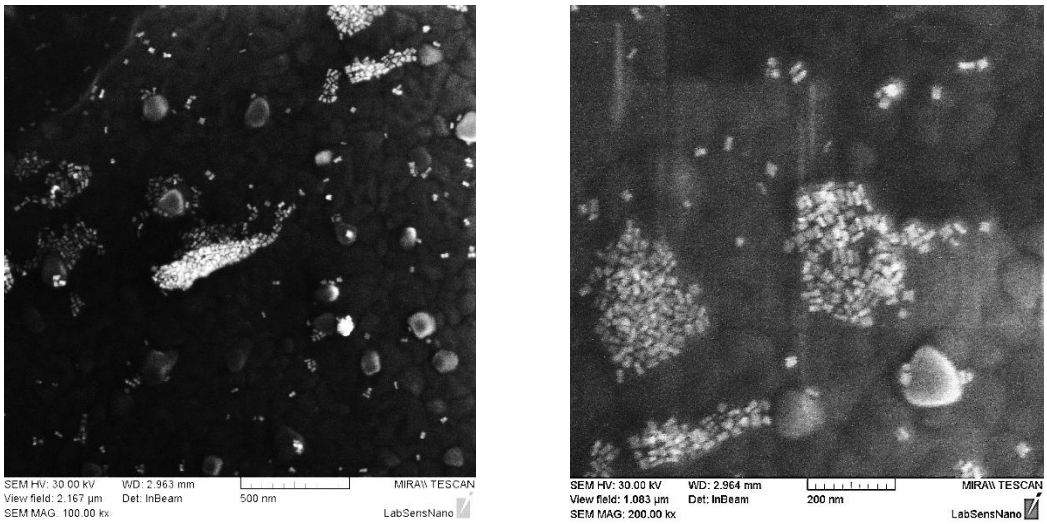

Figure 36 SEM image of sample 5: gold nanorods at magnification 100 nm (left) and 200 nm (right)

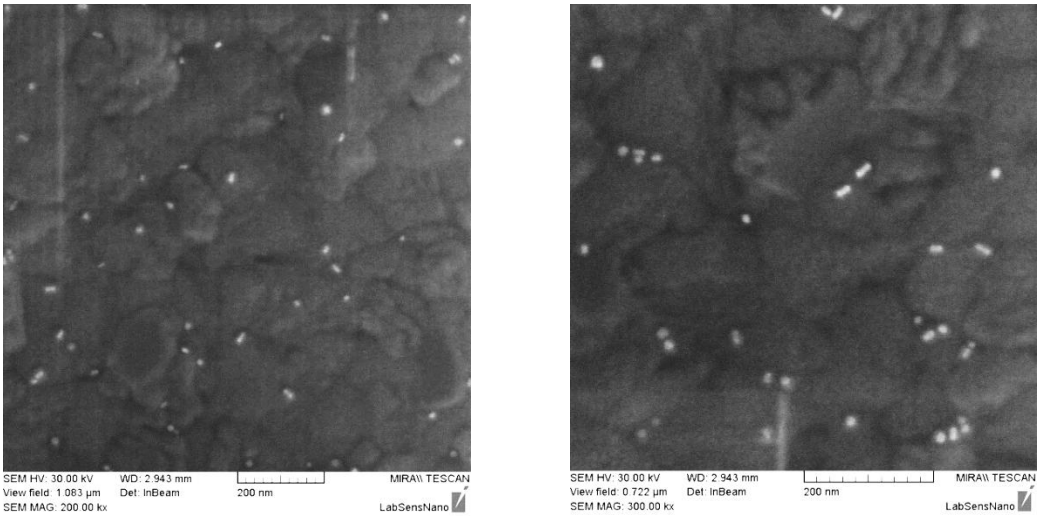

Figure 37 SEM image of sample 6: gold nanorods at magnification 100 nm (left) and 200 nm (right)

DLS analysis was used to confirm the SEM and UV-VIS results of AuNRs size distribution and concentration. Based on the size distribution, it is obvious that AuNPs of two different sizes were represented in every sample. The presence of 1 nm particles, which could not be recognised by SEM due to very small dimension, and particles of 40–50 nm was found out by DLS analysis (Figure 38). From volume distribution (Figure 39) it can be seen that the small particles intensity was much greater than the intensity of the larger ones. It indicates that small particles of about 1 nm are represented in much higher distribution than those of about 40–

50 nm. DLS analysis confirmed the SEM assumption that the sample 5 has the highest concentration of AuNRs with diameter of about 30 nm (Figure 39).

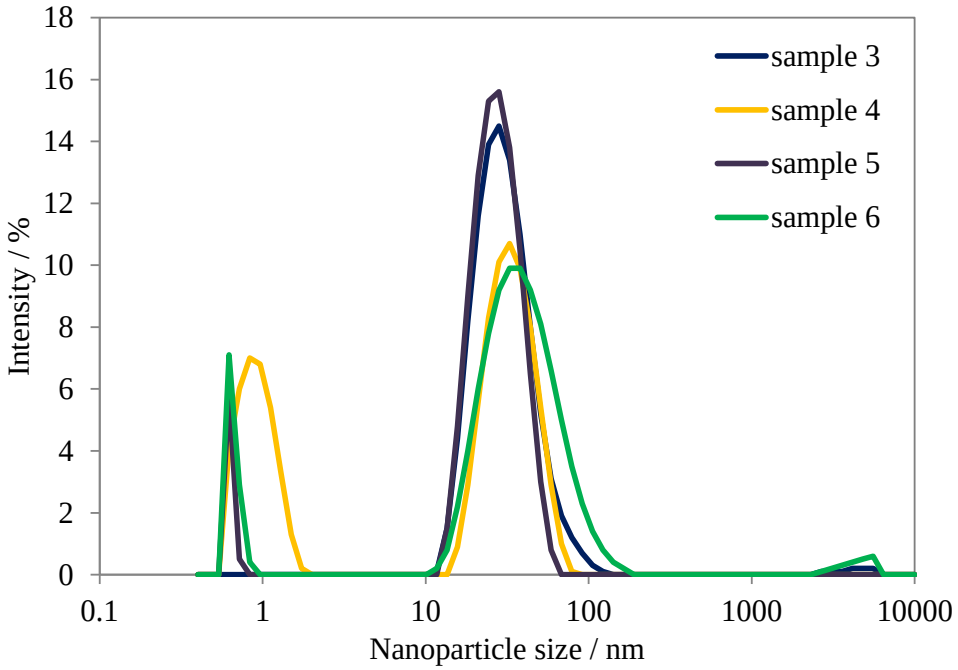

Figure 38 DLS analysis of AuNRs prepared with various amount of added seed (50 –160 µL): size distribution

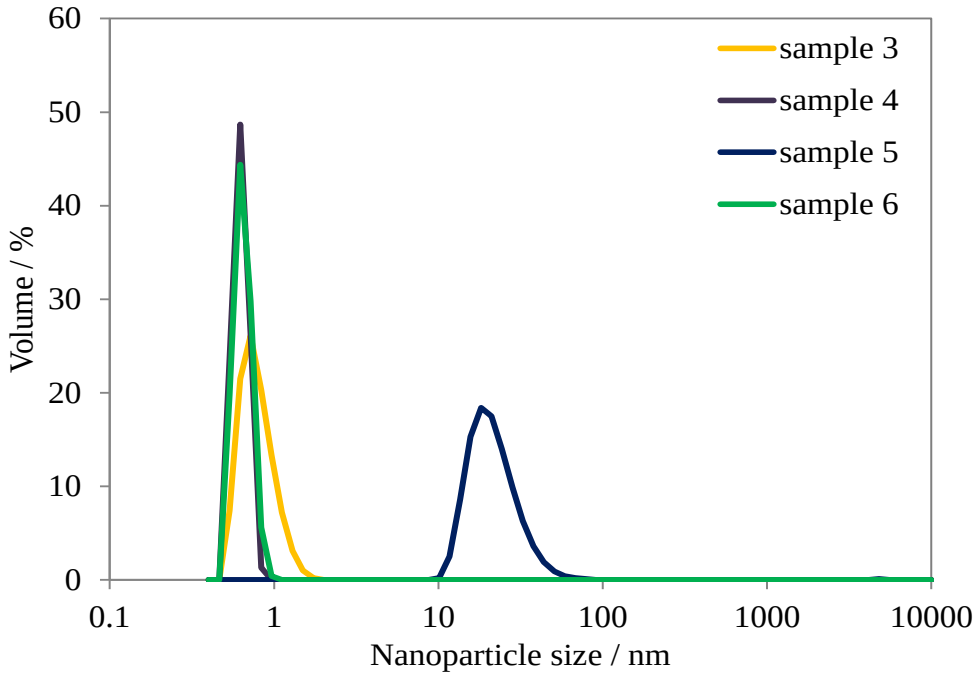

Figure 39 DLS analysis of AuNRs prepared with various amount of added seed (50 µL–160 µL): volume distribution

8.4.2. Influence of HAuCl4 concentration

Three samples with different conditions were prepared to compare the influence of gold salt concentration on the final product (Table 3). The best AR results were gained with the lowest investigated concentration, namely 0.001 M (sample 5). More robust AuNRs were synthesized by using higher concentrations. In these cases, the final products were obtained from supersaturated gold solution.

Table 3 Evaluation of samples with different c[$HAuCl_4.3H_2O$]

Sample	c[$HAuCl_4$]/M	c[$AgNO_3$]/M	Seed /µl	Width/nm	Length/nm	AR	λ_{max}/nm
1	0.01	250	120	25	40	1.6	620
2	0.005	250	120	30	40	1.4	624
5	0.001	250	120	8	25	3.1	632

By comparing the UV-VIS spectra of particular samples, it was found that the best result was obtained for sample with the lowest $HAuCl_4$ concentration (Figure 40). The fact indicated that the AR of the sample would be the highest. The spectrum showed a significant response at the spectra beginning. Due to the lower pH (2.57), it was probably caused by oversaturation of growth solution by ascorbic acid. Low absorption of the other samples was likely a consequence of the samples dilutions due to their gold oversaturation.

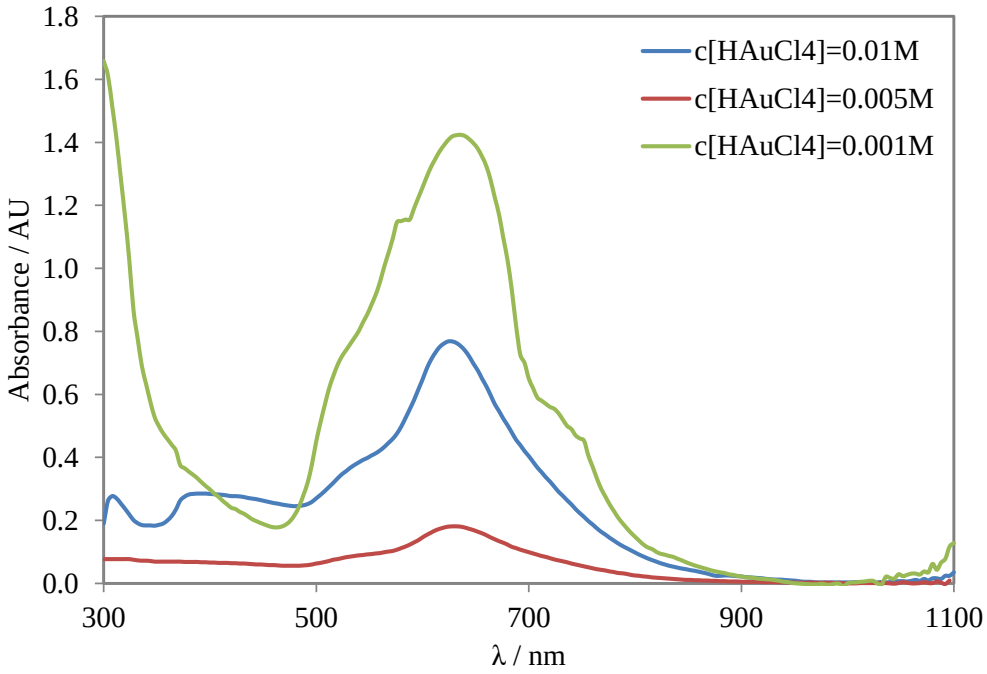

Figure 40 UV-VIS spectra of AuNRs formed with different c[$HAuCl_4.3H_2O$]

According to SEM analysis, the biggest and the robustest AuNRs were prepared with the highest concentration of $HAuCl_4$ (Figure 41). In this case, the highest NRs concentration was also obtained. It was proved, that the AuNRs length and also the width decreased with decreasing $HAuCl_4$ concentration (Figure 42). In contrast, SEM analysis confirme the assumption from UV-VIS analysis, i.e. the biggest AR was obtained from the lowest $HAuCl_4$ concentration (Figure 43). Due to the smallest size, the AR of the sample prepared with the lowest gold concentration was also evaluated by TEM analysis for more detailed view (Figure 44). All solutions were almost monodisperse, however small amount of NSs and nanocubes (NCs) was presented as well (e.g. Figure 41).

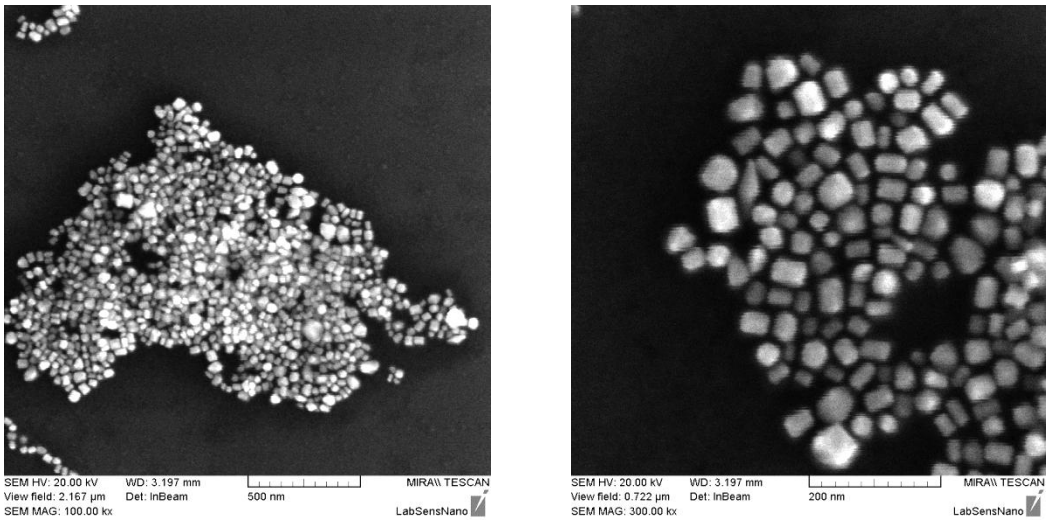

Figure 41 SEM image of sample 1: gold nanoparticles, mostly gold nanorods with a small amount of gold nanocubes and nanospheres at magnification 100 nm (left) and 300 nm (right)

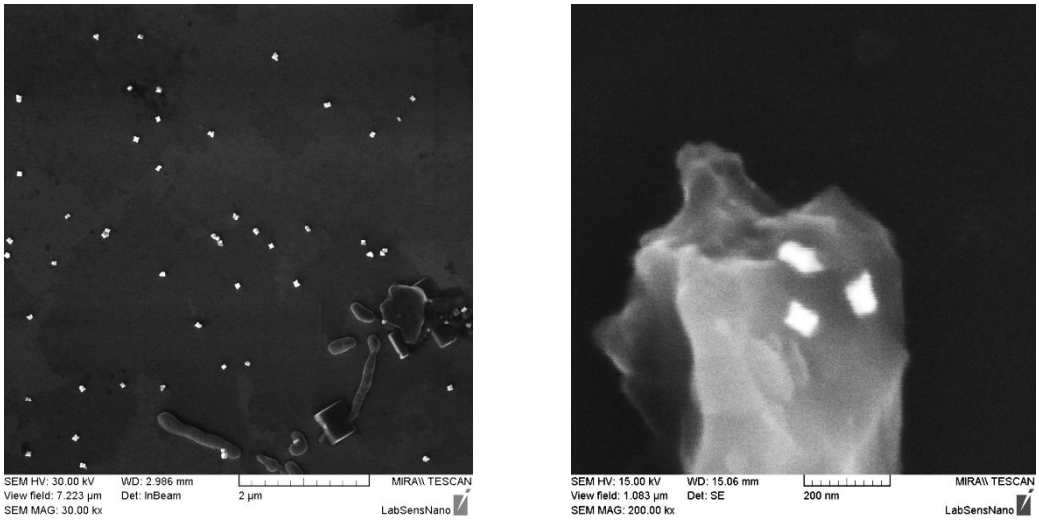

Figure 42 SEM image of sample 2: gold nanorods at magnification 30 nm (left) and clearly visible CTAB cover with three AuNRs at magnification 200 nm (right)

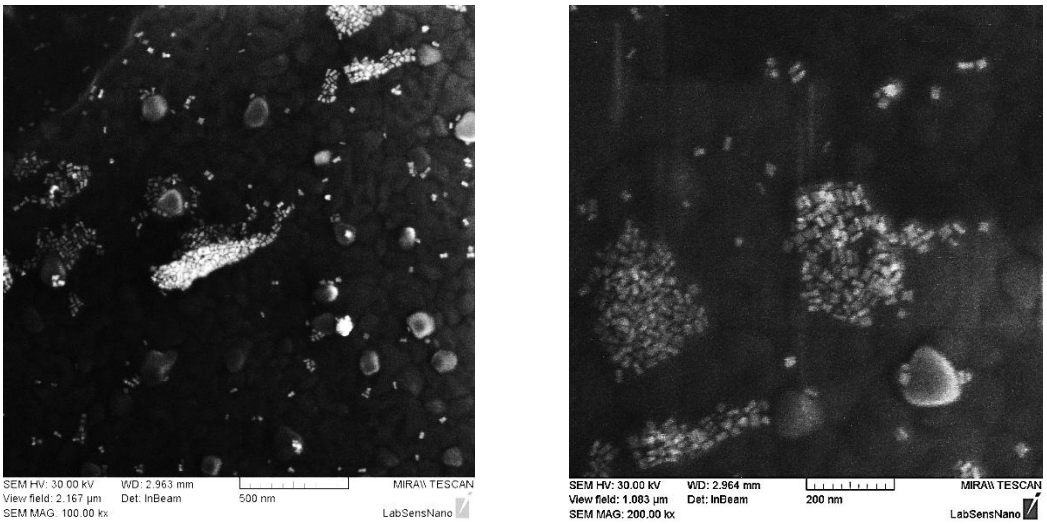

Figure 43 SEM image of sample 5: areas with a large concentration of AuNRs at magnification 100 nm (left) and 200 nm (right)

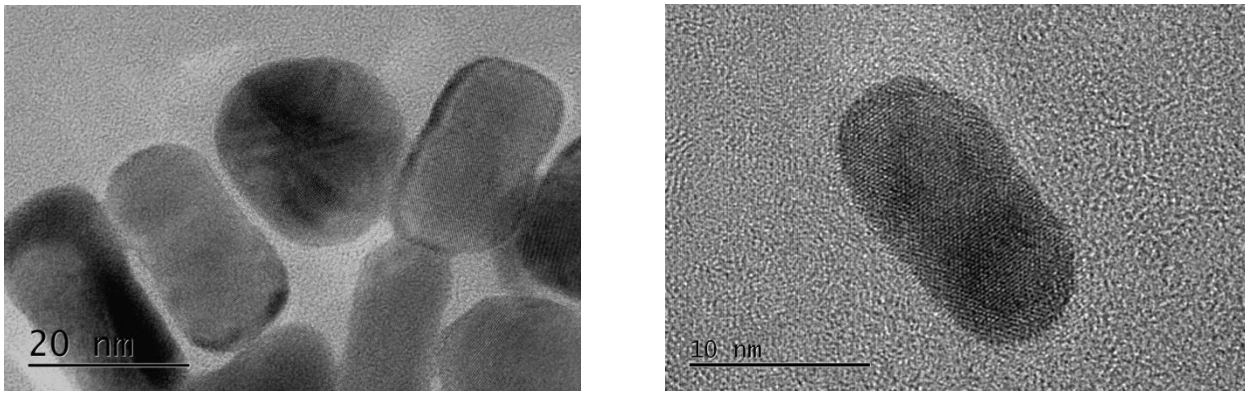

Figure 44 TEM images of sample 5: solution containing AuNRs with uniform ARs of 2 and rarly presented nanospheres, scale bars: 20 nm (left) and 10 nm (right)

Based on SEM and TEM images, the estimated particles size was around 40 nm for the samples 1 and 2, and 15–20 nm for sample 5. DLS analysis proved that samples 1 and 2 contained AuNPs of about the same size in the range of 40–250 nm (Figure 45, Figure 46). The expectation that sample 5 contained the smallest NPs was established by comparing the results from DLS. DLS volume distribution confirmed that the NRs in sample 1 (visible in Figure 41) were the most represented in the final product in the same size (Figure 46). It indicates that this solution was highly monodispersed, with an size average of 30–40 nm. In the other cases, the most nanoparticles were prepared in size of about 5–10 nm.

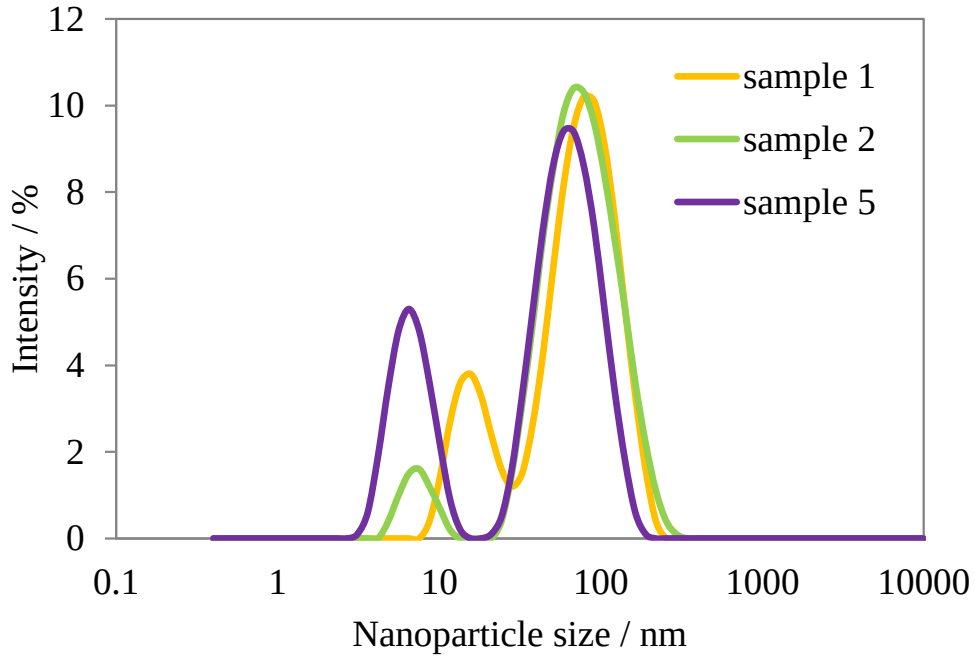

Figure 45 DLS analysis of AuNRs formed with different c[$HAuCl_4.3H_2O$]: size distribution

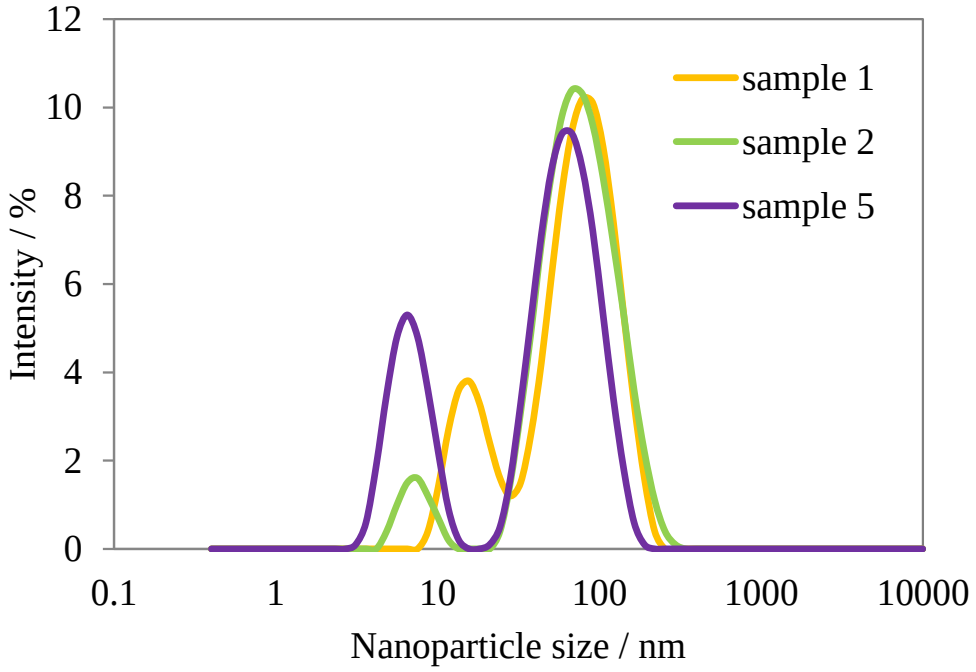

Figure 46 DLS analysis of AuNRs formed with different c[$HAuCl_4.3H_2O$]: volume distribution

8.4.3. Influence of AgNO3 concentration

The combination of silver and bromid alters the shape of CTAB micelles. It follows that the silver concentration is an important factor influencing mainly the AR of NRs. The prerequisite is that AR increased by increasing silver concentration [41]. The dependence of AR

on $AgNO_3$ concentration was investigated using four samples prepared under different conditions (Table 4).

Table 4 Evaluation of AuNRs prepared with different c[$AgNO_3$]

Sample	c[$HAuCl_4.3H_2O$]/M	Seed/µL	c[$AgNO_3$]/µL	Width/nm	Length/nm	AR	λ_{max}/nm
7	0.001	50	150	16	35	2.2	628
3	0.001	50	250	13	35	2.7	628
8	0.001	50	350	8	35	4.3	640
9.	0.001	50	450	11	26	2.4	616

According to UV-VIS spectra, increasing $AgNO_3$ addition caused the red-shift of LPR maximum gradually until the concentration in solution had not exceeded the critical volume of 350 µL. Further increase of concentration caused a blue shift of the LPR maximum position (Figure 47).

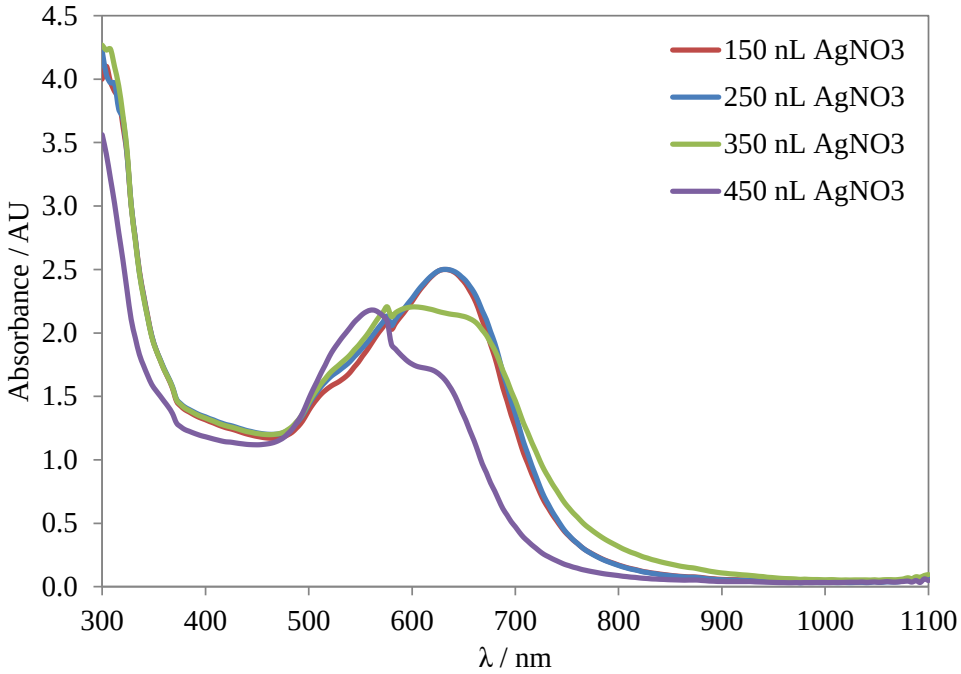

Figure 47 UV-VIS spectra of AuNRs formed with different $AgNO_3$ amount

The prepared AuNRs were analyzed by SEM to observe their distribution, size and shape. The above mentioned hypothesis based on UV-VIS spectra was proved. It means, that until the

critical amount of 350 µL, the AuNRs length stayed the same, but the width decreased with increasing amout of added $AgNO_3$ (Figure 48–Figure 51). It follows that the AR increases. Further increase of concentration results in AuNRs with bigger width thereby reducing AR (Figure 51). The quantity of prepared AuNRs had the same dependence on $AgNO_3$ concentration as AR – the highest amount was obtained after addition of 350 µL $AgNO_3$ (Figure 50).

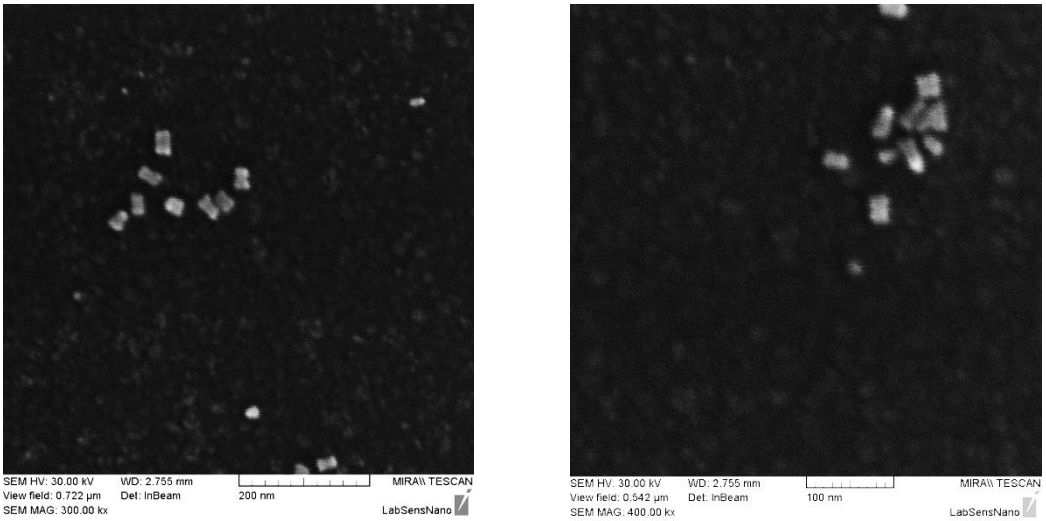

Figure 48 SEM images of sample 7: gold nanorods at magnification 300 nm (left) and 400 nm (right)

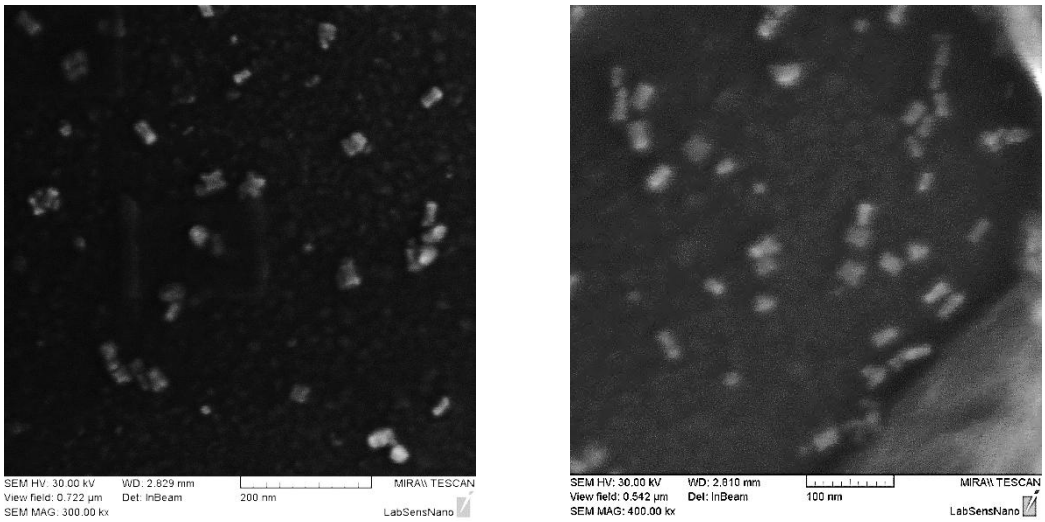

Figure 49 SEM image of sample 3: gold nanorods at magnification 300 nm (left) and 400 nm (right)

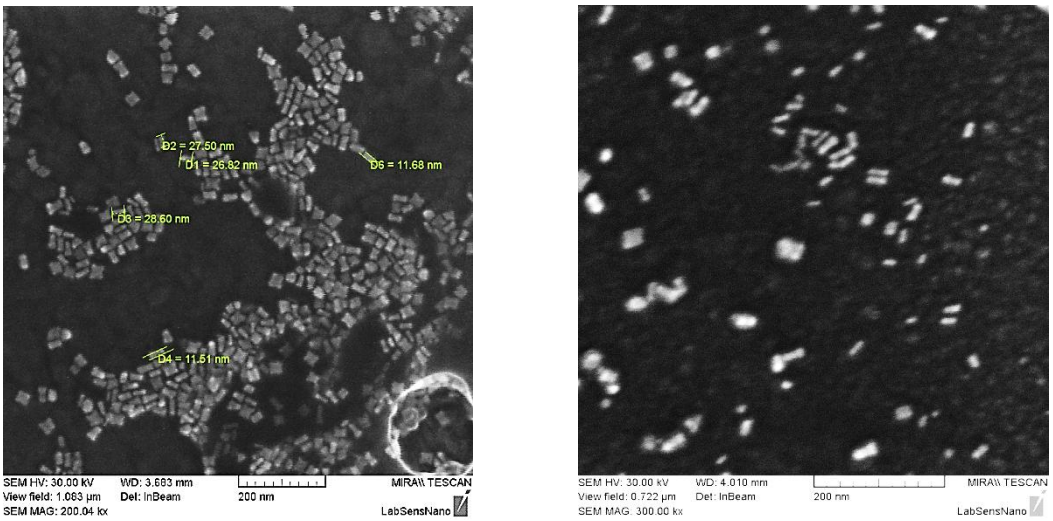

Figure 50 SEM images of sample 8: gold nanorods at magnification 200 nm (left) and 300 nm (right)

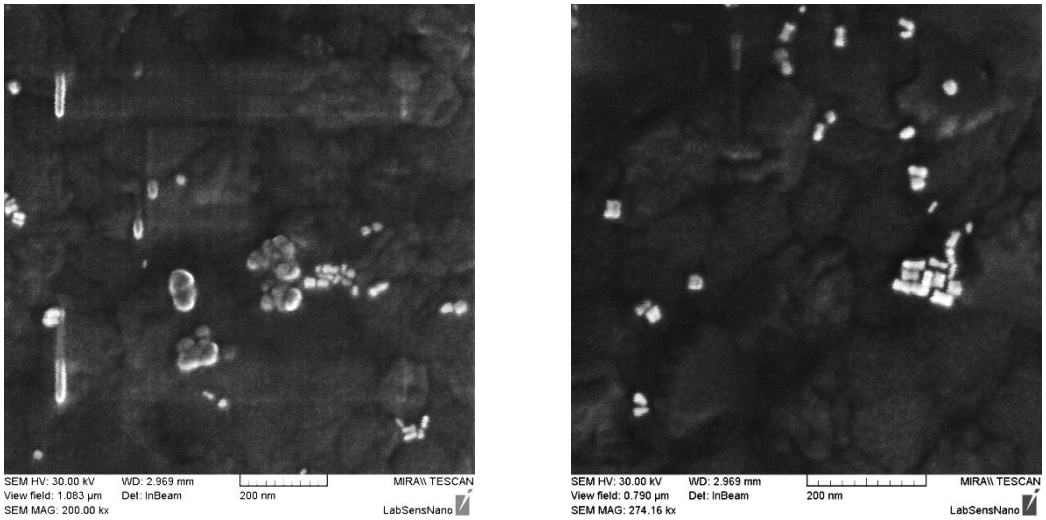

Figure 51 SEM images of sample 9: gold nanorods at magnification 200 nm (left) and 300 nm (right)

The SEM and UV-VIS results were supported by DLS analysis which proved that the final product made by addition of 350 µL silver salt has the highest size distribution of AuNRs of about 30 nm (Figure 53). DLS analysis also showed that all samples contained AuNPs of about the same size in the range of 40–250 nm (Figure 52). Size distribution supported by volume distribution revealed the presence of 1 nm particles, which could not be recognised by SEM due to low resolution of this tool (2 nm). Based on the volume distribution, it is evident that the small articles are much more represented than the larger ones.

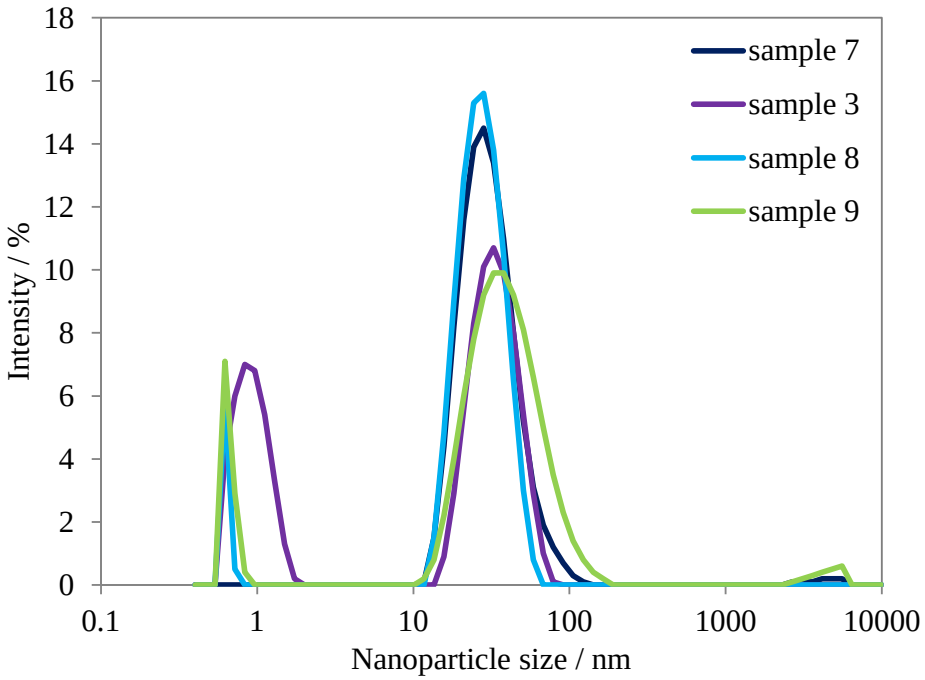

Figure 52 DLS analysis of AuNRs prepared with different c[$AgNO_3$]: size distribution

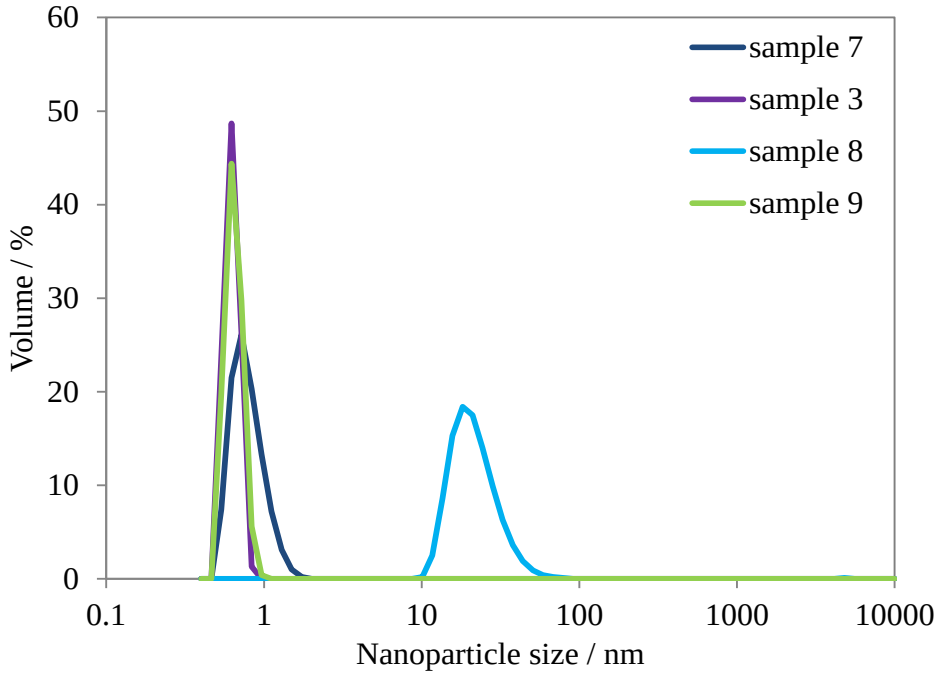

Figure 53 DLS analysis of AuNRs prepared with different c[$AgNO_3$]: volume distribution

8.4.4. EDX characterization of AuNRs

EDX analysis was used to ensure that bright crystals which can be seen on SEM images really corresponded to the AuNPs. There was a problem with EDX analysis relating to very small AuNRs size which could not be detected precisely by EDX detector. It was necessary to find bigger gold clusters for using the EDX analysis. Based on DLS analysis, the samples with NPs size bigger than 100 nm were choosen for further EDX characterization. Finally, the EDX analysis was performed on the sample 9. The EDX point scan has shown the element distribution in the solution (Figure 54, Figure 55). A large representation of gold can be observed from the image below. In addition, the EDX mapping (Figure 56) provides a meaningful picture of the elements distribution on the surface compared to the conventional SEM image. The elements such as carbon (C), oxygen (O) and bromine (Br) were detected indicating the presence of CTAB residues. Titanium (Ti) was used as substrate, where the analyses were performed.

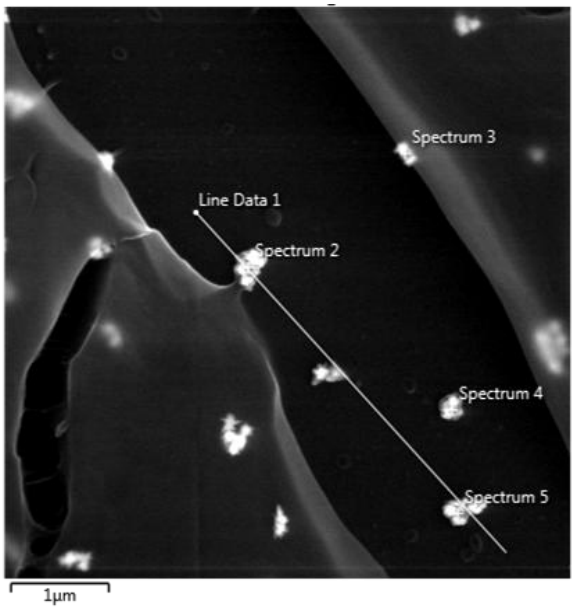

Figure 54: SEM image of sample 9 for the EDX point scan

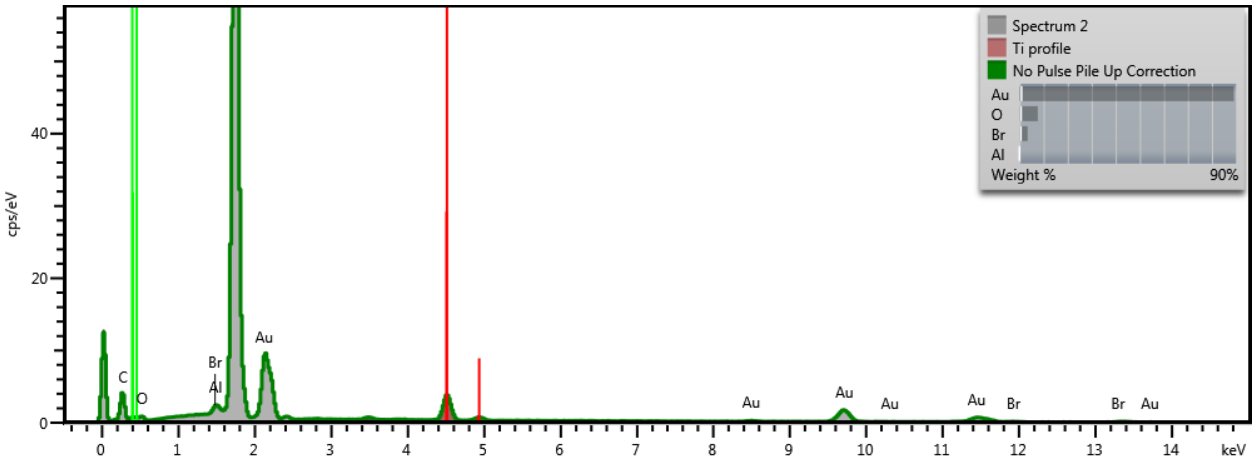

Figure 55: EDX analysis of AuNRs, point scan of sample 9

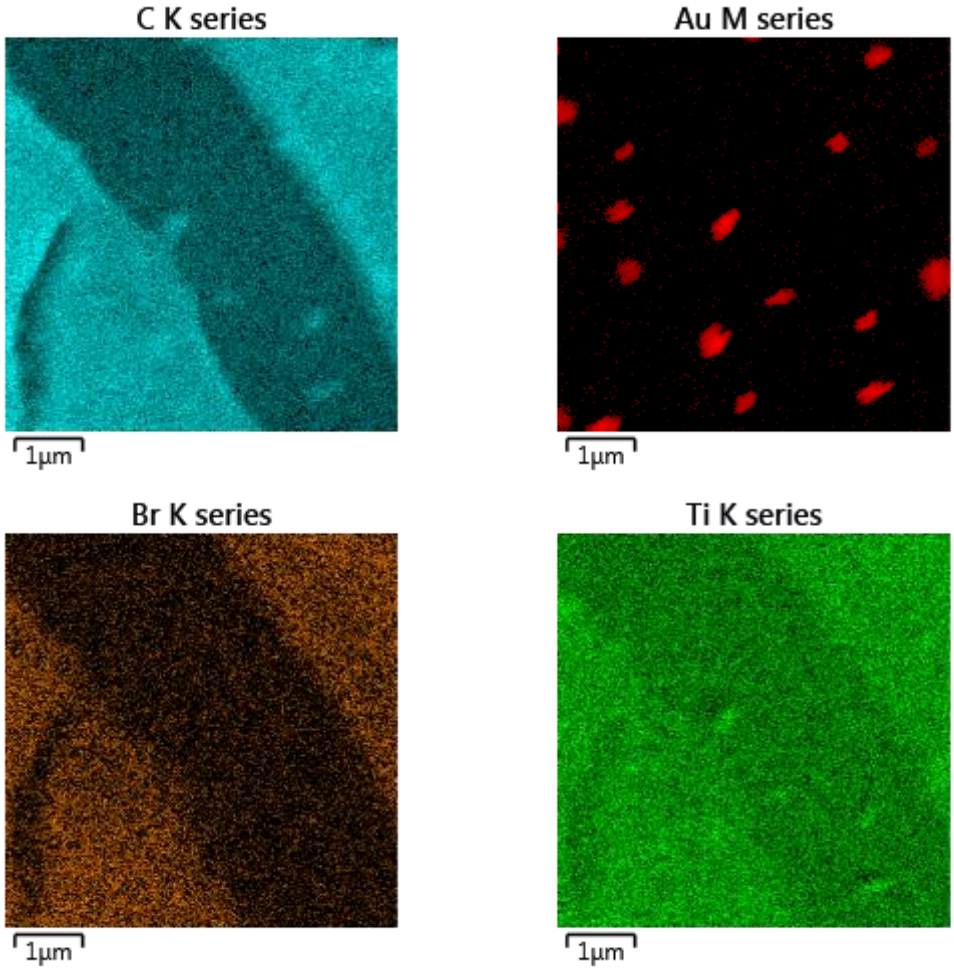

Figure 56: EDX mapping of sample 9: elements distribution on the surface - carbon (C), oxygen (O), bromine (Br) and titanium (Ti)

8.4.5. Final summary of reagents influence on AuNRs

The effect of various reagents concentrations on the AuNRs formation and properties was investigated by the analysis of AR and absorption maximum of all samples. It was necessary to normalize the real values of reagent concentration (Table 5) as well as AR (Table 6) and absorption maximum of AuNRs (Table 7) to obtain adequate and comparable dependencies of concentration influence of single reagents.

Table 5 Conversion table of real concentration values (RV) on normalized (NV)

	SEED concentration		$HAuCL_4$ concentration		$AgNO_3$ concentration	
NV of concentration	RV / µL	NV	RV / M	NV	RV / µL	NV
1	50	1	0.010	3	150	1
2	80	2	0.005	2	250	2
3	120	3	0.001	1	350	3
4	160	4			450	4

Based on the obtained results, it can be said that the AuNRs with the highest AR would be prepared with the lowest tested amount of added seed (50 µL), the lowest tested concentration of $HAuCl_4$ (0.001 M) and the second highest tested amount of $AgNO_3$ (350 µL). In contrast, the worst final product would be gained by the highest tested amount of added seed (160 µL), the second tested concentration of $HAuCl_4$ (0.005 M) and again by the second highest tested amount of $AgNO_3$ (350 µL) (Figure 57).

Table 6 Conversion table of real AR values (RV) on normalized (NV)

	SEED AR		$HAuCL_4$ AR		$AgNO_3$ AR	
NV of concentration	RV	NV	RV	NV	RV	NV
1	1.9	4	1.6	2.5	2.2	1
2	1.4	2	1.4	1.0	2.7	3
3	1.6	3	3.1	4.0	4.3	4
4	1.3	1			2.4	2

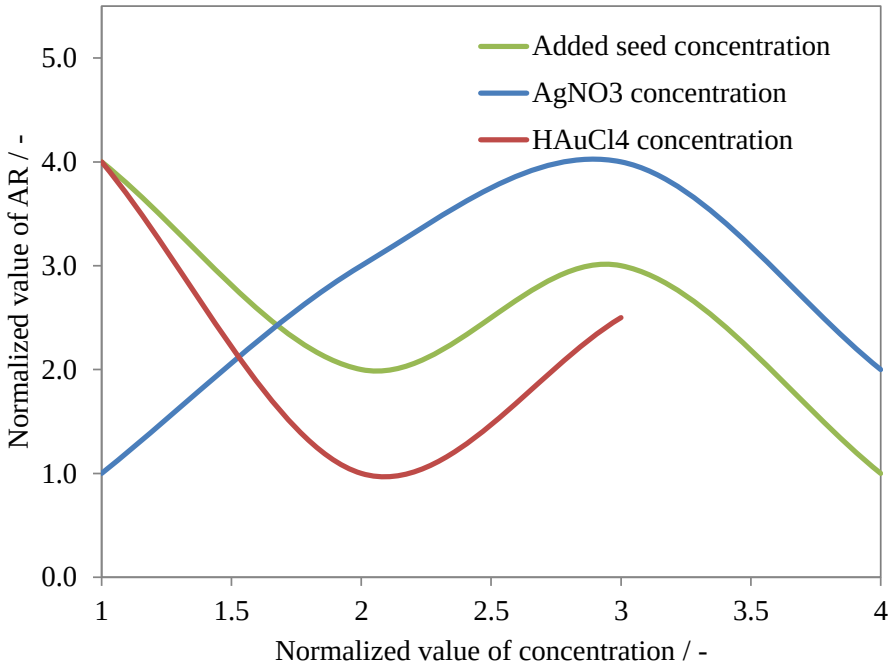

Figure 57 Dependence of concentration change of various reagents on the AR size

The LPSR is closely related to AuNRs size. The assumption was that the position of maximum absorbance would increase with increasing AR. Based on the results the expectation was confirmed and the influence of single reagent concentration was the same as in previous case with AR (Figure 58).

Table 7 Conversion table of real absorption maximum values (RV) on normalized (NV)

	SEED λmax		$HAuCL_4$ λmax		$AgNO_3$ λmax	
NV of concentration	RV / nm	NV	RV / nm	NV	RV / nm	NV
1	632	3	620	1	628	2
2	624	2	624	3	628	2
3	632	3	632	4	640	4
4	616	1			616	1

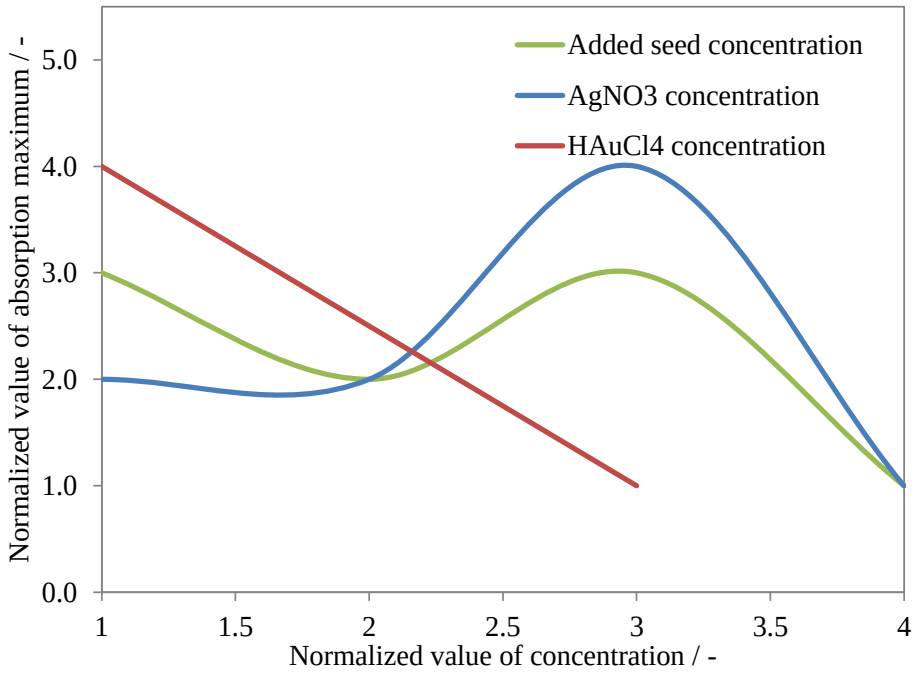

Figure 58 Dependence of concentration change of various reagents on the absorption maximum

8.5. Characterization of modified AuNRs

8.5.1. TEOS coated AuNRs

Mesoporous silica was selected for use as a coating material for AuNRs due to highly biocompatibility and stability in biological environments. UV-VIS spectra showed LPSR shift to lower values after the modfication (Figure 59). The reason of peak shift became clear after the SEM evaluation which revealed the presence of AuNRs clusters covered with TEOS layer

(Figure 60). The cluster formation could be caused by insufficient NPs washing or bad pH during the modification.

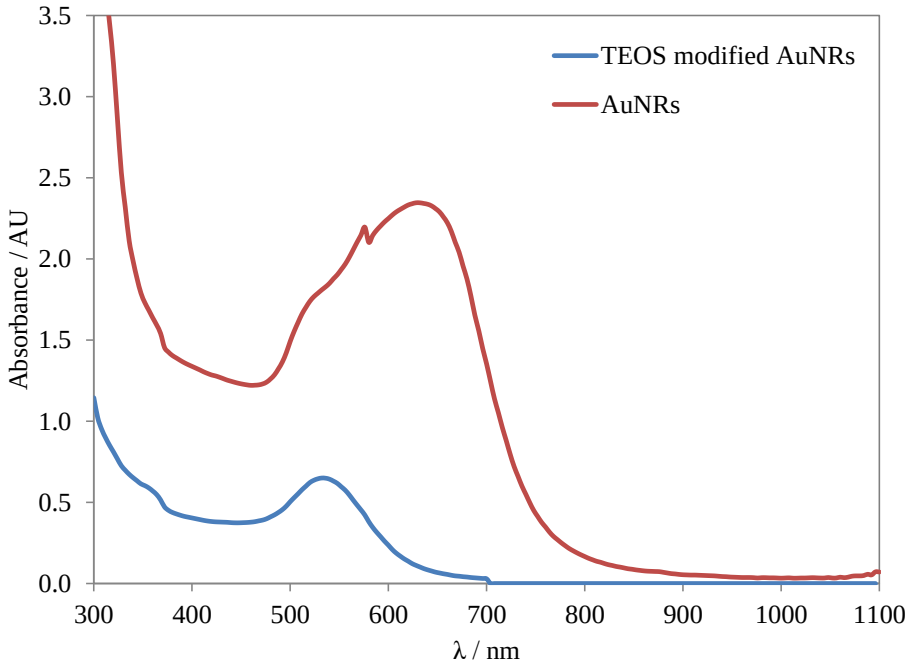

Figure 59 UV-VIS spectra of AuNRs and TEOS-AuNRs: absorbance change of AuNRs after modification with TEOS

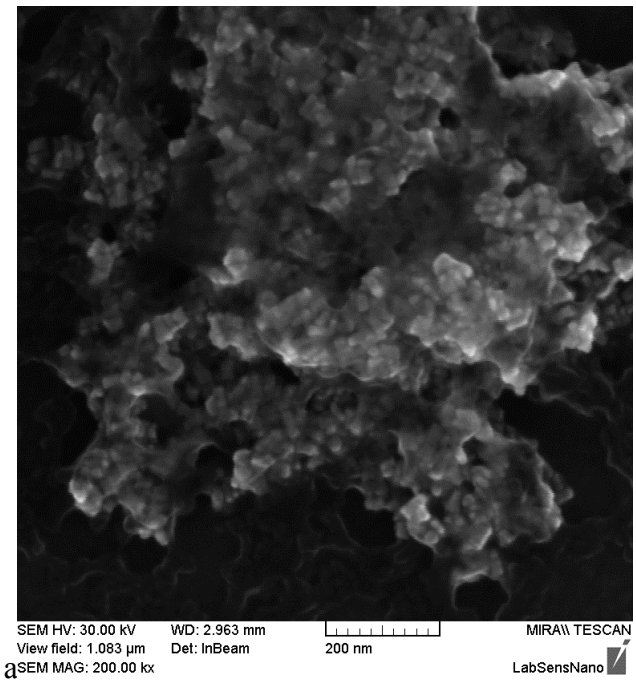

Figure 60 SEM image of modified gold nanorods with TEOS at 200 nm magnification: gold nanorods aggregation are visible under a layer of TEOS

8.5.2. PEG coated AuNRs

Thiol-terminated polyethylene glycol (PEG) was used to functionalize the AuNRs surface in order to improve their in vivo stability and decrease their cytotoxicity. Two modifications of the same AuNRs (sample 9) differing from each other in the amount of added PEG were tested. UV-VIS spectra showed that the absorbance of AuNR significantly decreased after the modification with PEG (Figure 61). It could be caused by lower concentration of PEG-AuNRs due to multiple washing after modification.

Table 8 Evaluation of AuNRs modification with different c[PEG]

	Concentration/ mg/10 mL	λ_{max}/nm
PEG 1	2.1	616
PEG 2	3.0	616

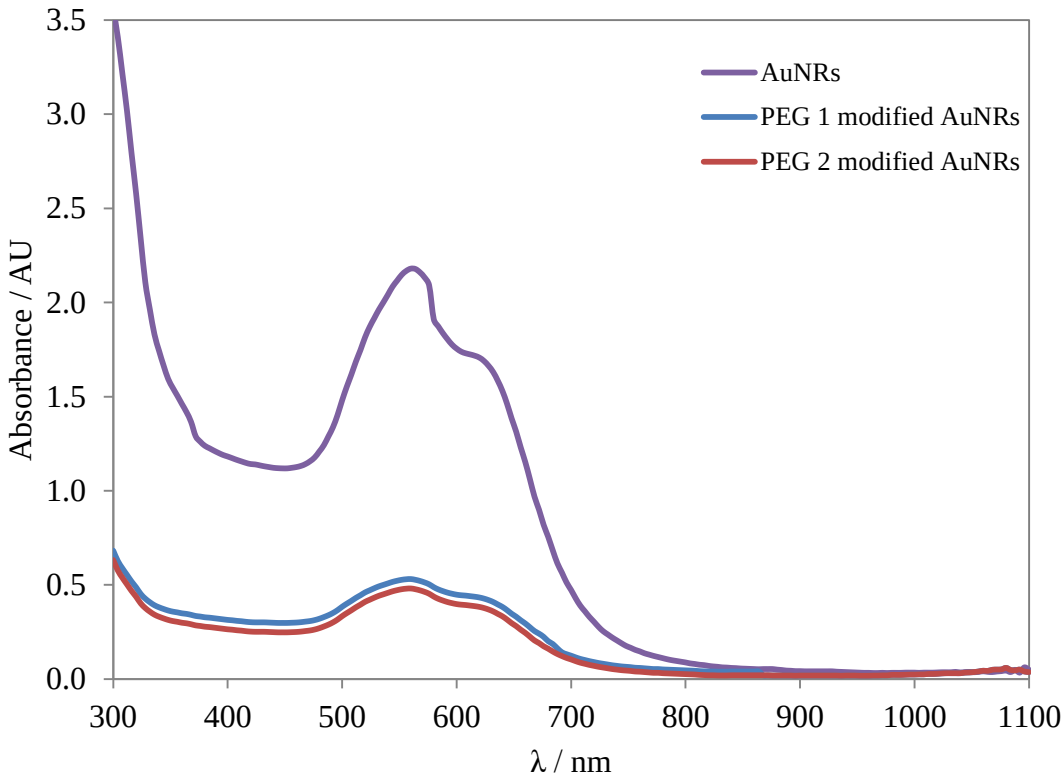

Figure 61 UV-VIS spectra of AuNRs (sample 9) and AuNRs with PEG cover

It was expected that it would not be significant difference in size between CTAB-AuNRs and PEG-AuNRs. The assumption was confirmed by the SEM and TEM analysis. SEM

evaluation showed visible AuNRs core coated with PEG (Figure 62). TEM observation provided a detailed view and reaffirmed SEM results (Figure 63).

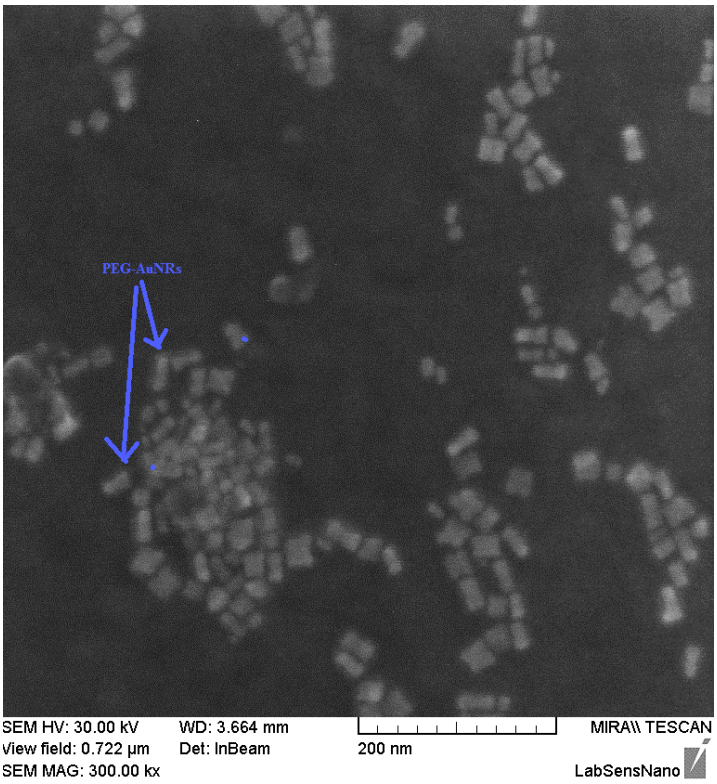

Figure 62 SEM image of modified gold nanorods with PEG at 300 nm magnification: thin PEG cover around gold nanorods is shown by blue arrows

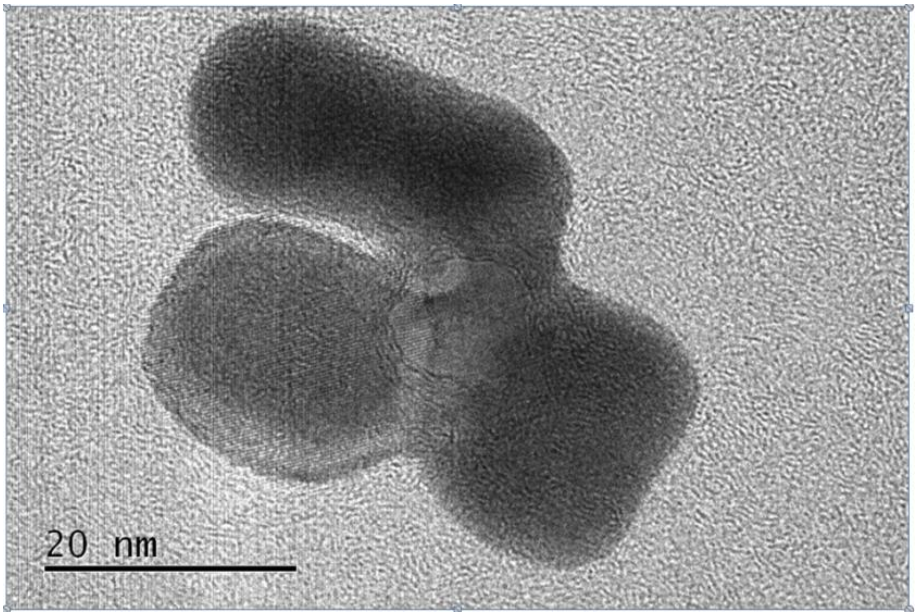

Figure 63 TEM images of gold nanorods functionalized with PEG

The presence of PEG was tested based on the knowledge about FTIR spectrum of PEG (Table 9, Figure 65). It was necessary to have a dried AuNPs for the analysis because colloidal solution contained lot of water which has high adhesion to the surface, unlike dispersed nanoparticles, and its spectrum drowned out the spectrum of NPs. Two different techniques how to get the dried NPs were tried. The first one was classic approach at elevated temperature. The centrifuged NPs were dried for three days at 80 °C in dryer. Nevertheless, the yield was very small and there was a problem with NPs separation from substrate they were dried on. The second technique was to dry AuNRs by using the lyophilization (Figure 64). This method how to get dried NPs was much faster, simpler and more efficient than the traditional method of drying NPs at elevated temperature. The problem was that the final product also contained a big amount of dried CTAB.

Figure 64 Photo of obtained NPs yield using lyophylization: sample 9 with (right) and without (left) PEG modification

The successful modification was confirmed by comparing final FTIR spectrum of PEG modified AuNRs with reference PEG spectrum. The identical peaks, were presenting in all cases (Figure 65). Mainly, the peak around 1110 cm^{-1} (C-O vibrations in ethers) is the most decisive indicator in the evaluations of PEG spectra. The presence of the peak is complies completely with PEG presence, because the other possible reagents, mainly CTAB, does not absorb in this region.

Table 9 PEG-capped FTIR spectrum [65]

Bound	Wavenumber / cm^{-1}
$-CH_2$ stretching	2.850–3.000
N–H bending	1.631
C=O stretching	1.660
C–H bending; $-CH_2$ and $-CH_3$	1.380
C–O–C stretching	1.100
N–H wagging	600–900

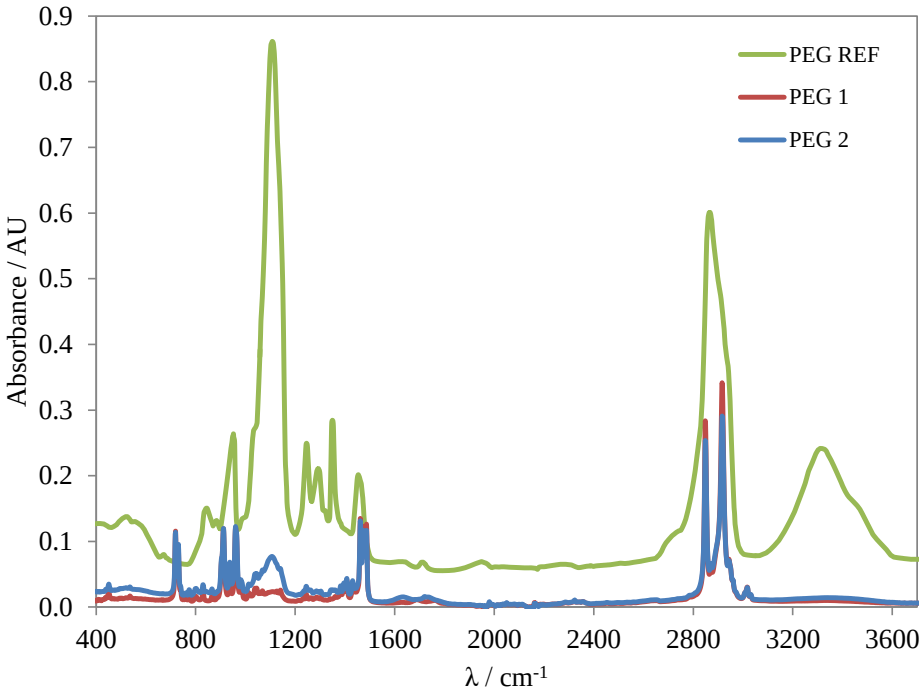

Figure 65 FTIR spectra of PEG modified AuNRs compared with reference FTIR spectrum of PEG

8.6. Evaluation of AuNRs cytotoxicity

The MTT viability assay was performed to estimate the cytotoxicity of three AuNRs samples to HEK 293 cell line. The influence of PEG modification on cells viability improvement was tested. Three different AuNRs concentrations (50, 100 and 200 μg/mL) each having three replicates wells were investigated in the experiment (Table 10). Viability was determined by absorption amount at 560 nm.

Table 10 Evaluation of viability

	PEG concentration / mg/10 mL	Concentration / μg/mL	Absorbance Average / AU	Viability / %
Sample 9	0	200	0.1367	34.84
		100	0.1367	44.47
		50	0.3133	61.93
Sample 9	2.1	200	0.2344	59.73
		100	0.2996	76.35
		50	0.3533	90.04
Sample 9	3	200	0.2267	57.78
		100	0.2621	66.80
		50	0.3655	93.14

Input logical assumption was that the lower used AuNRs concentration caused the lower toxicity. It follows that the highest cell viability should be at the lowest AuNRs concentrations. The expectation was confirmed by the MTT test (Figure 66). Based on the results, the highest cells viability was performed by the lowest tested concentration of each sample. It was also predicted that the higher concentration of PEG brought about the higher cells viability (Figure 67). Pursuant to the results, the highest viability was performed by the highest PEG concentration, in contrast with the lowest viability caused by the non modified AuNRs. The toxicity level of substances under the experimental conditions, at a given time and in a given cell type could be represented by the IC50 (half maximal inhibitor concentration). It is the concentration of noxae, which produces 50% of the maximum cell death. The lower toxicity is exhibited by the lower IC50. Consequently, non modified AuNRs at concentration higher than 70 μg/mL caused 50% cell death. In contrast with PEG modified AuNRs, where the IC50 was much bigger than the tested concentrations.

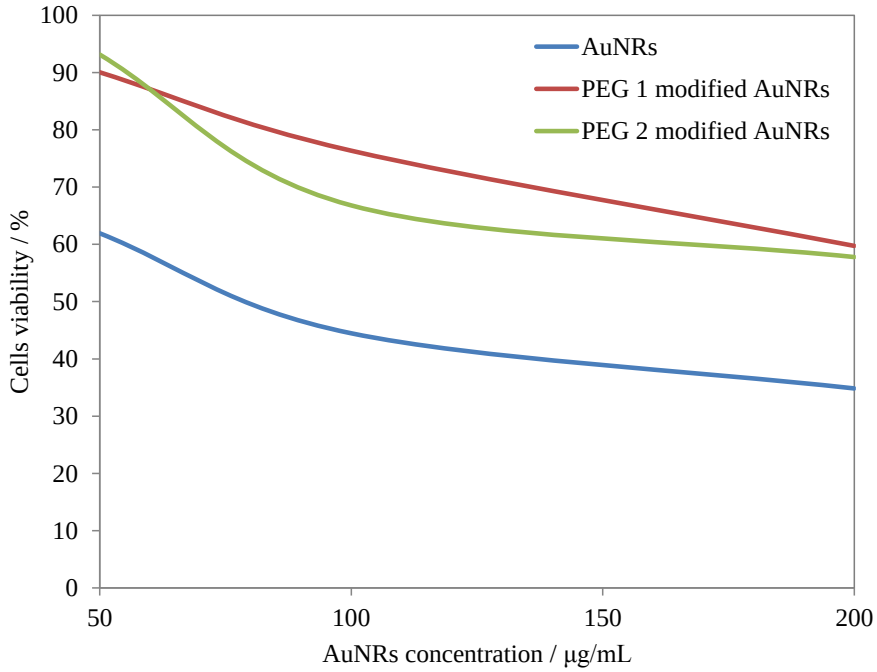

Figure 66 Depenence of HEK 293 cells viability on different concentrations of AuNRs and PEG-AuNRs determined by MTT test

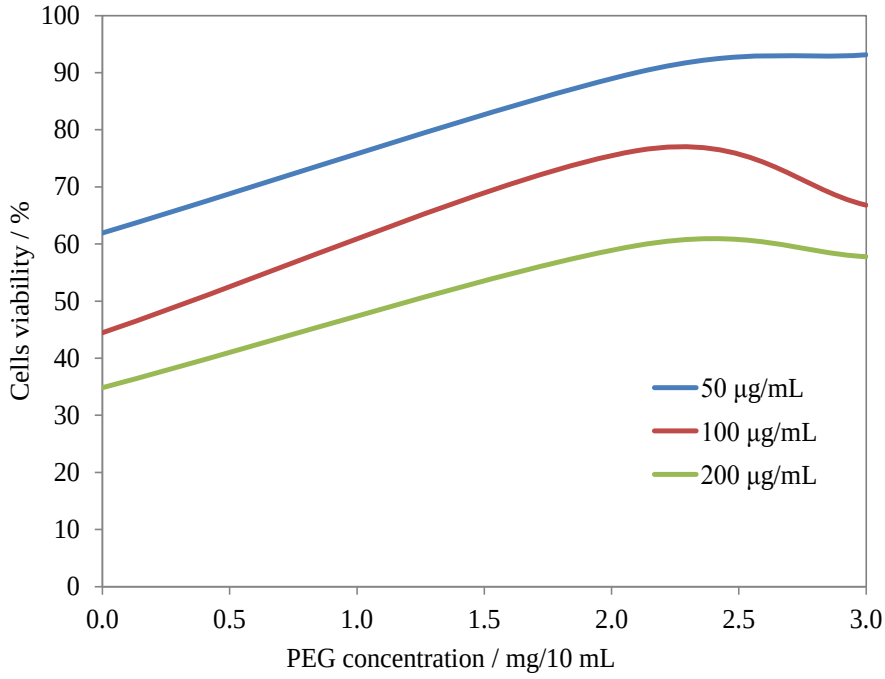

Figure 67 Depenence of cells viability on PEG concentration for different concentration of AuNRs

9. Conclusion

In this work, the sedless growth method was used for the AuNRs preparation. The main aim was to create stable and monodiperse colloidal solution containing uniform and biocompatible AuNRs. Their final chemical and physical properties were examined with respect to possible further biomedical applications, mainly photothermal therapy.

The AuNRs were prepared by addition of small spherical AuNPs representing seed solution to growth solutions. Growth solution usually contained gold salt, surfactant and reducing agent. AuNRs were synthesized by using CTAB as a surfactant. CTAB is very appreciated not only as an essential component in the anisotropic AuNRs growth but also for the subsequent AuNRs stability guaranteed by noncovalent coating. There was a few problems that needed to be solved during the AuNRs preparation. In the first instance, it is the stability and solubility of CTAB solution. For AuNRs preparation, saturated aqueous solution of CTAB was used. The solution needed to be well dissolved by heating to at least 26 °C (Krafft point of CTAB) in warm water bath. The Krafft point is the minimum temperature at which surfactant forms micelles which are necessary for AuNRs growth. The problem of stability is also related to temperature. CTAB aqueous solution tends to create aggregates at room temperature. This fact could complicate the futher AuNRs stability because the surfactant is largely presented in the final product. There were two methods how to keep the AuNRs final solution stable. The first possibility was to centrifuge fresh prepared AuNRs suspension immediately after AuNRs preparation and remove the transparent supernatant portion. The second option was to keep the final product at elevated temperature (~ 27 °C) which ensured that the CTAB stayed dissolved. The next problem was the toxicity of CTAB. Free CTAB is known to be highly cytotoxic for cells. In order to remain CTAB coated rods soluble, it is necessary to retain the concentration of free CTAB in solution above a certain value. This could be achieved by AuNRs centrifugation or modification with PEG and TEOS.

The final AuNRs were obtained by various processes. The influence of three basic reagents, namely the concentration of $HAuCl_4$ and $AgNO_3$ in growth solution and the amount of added seed on the final product was investigated. The synthesis conditions of AuNRs were modified in order to understand the influence of each reagent on the length, width, AR, and consequently the optical properties of prepared AuNRs. AR and absorption maximum of AuNRs played an important role of investigated endpoints. It was found out that the best results in the form of the highest NPs ARs and LPSR were obtained by the smallest seed addition together

with the smallest concentration of $HAuCl_4$. and with $AgNO_3$ amount of 350 μL. It was also confirmed that the AR was very closely related to LPS and it exists almost linear dependece between them.

The final product was modified with TEOS and PEG mainly in order to improve its *in vivo* stability and decrease its cytotoxicity. The final product modified with TEOS showed worse properties than before the modification, particularly relating to very aggressive aggregation. It could be caused by inconvenient pH value during the modification. PEG-modification was tested at two different condiditons varying from each other in the amount of added PEG. The presence of PEG was tested based on the knowledge about FTIR spectrum of PEG, SEM and TEM analyses. The possibility of biomedical applications was demonstrated by MTT test. Dramatic biocompatibility improvement was performed by PEG modified AuNRs. The cell viability was increased with increasing concentration of PEG. It could be caused by similar reduction of the toxic effect of presented CTAB.

Very important result of this work is the separation of dried AuNRs from colloid solution by using the lyophilization. This method allows to get dried NPs in much faster, simpler and more efficient way than the traditional method of NPs drying at elevated temperature. The only problem was with presence of CTAB, which stayed in the sample after the lyophilization in dried form. This problem could be figured out by multiple washing of CTAB-NRs, but precisely need to be solved in future work.

In conclusion, the main outcome of this work is the synthesis of whole new spectrum of different sized gold nanorods, which were all almost uniform and monodisperse. Futhermore, the improvement of their biocompatibility for *in vivo* application was reachedby PEG modification which was also confirmed by MTT test.

The future progress of this work, specifically for the application in vitro, would be limited by the finding of conditions for red-shift of the longitudal plasmon. It is necessary to produce uniform, stable and biocompatible AuNRs with maximum absorption at ~700–1200 nm based on the knowledge about wavelength criterion, which is considered to be the best spectral region for imaging and therapy. After the fulfillment of this criterion, the PEG-AuNRs have potential not only for thermal therapy, but also for the targeted therapy and imaging. This made AuNRs one of the best candidate with multiple possibilities of applications in combating cancer.

10. References

[1] SEN, K. C. On the Stability of Colloidal Solutions. III. *The Journal of Physical Chemistry*, 1924, vol. 29, no. 5, pp. 517-539. ISSN 0092-7325.

[2] NG, V. W. K. et al. Gold: a versatile tool for in vivo imaging. *Journal of Materials Chemistry B*, 2013, vol. 1, no. 1, pp. 9-25. ISSN 2050-750X.

[3] HUANG, Y. et al. Biomedical nanomaterials for imaging-guided cancer therapy. *Nanoscale*, 2012, vol. 4, no. 20, pp. 6135-6149. ISSN 2040-3364.

[4] LOHSE, S. E. a MURPHY, C. J. The Quest for Shape Control: A History of Gold Nanorod Synthesis. *Chemistry of Materials*, 2013, vol. 25, no. 8, pp. 1250-1261. ISSN 0897-4756.

[5] PÉREZ-JUSTE, J. et al. Gold nanorods: Synthesis, characterization and applications. *Coordination Chemistry Reviews*, 2005, vol. 249, no. 17–18, pp. 1870-1901. ISSN 0010-8545.

[6] MURPHY, C. J. et al. The Many Faces of Gold Nanorods. *The Journal of Physical Chemistry Letters*, 2010, vol. 1, no. 19, pp. 2867-2875. ISSN 1948-7185.

[7] ALKILANY, A. M. et al. Gold nanorods: Their potential for photothermal therapeutics and drug delivery, tempered by the complexity of their biological interactions. *Advanced Drug Delivery Reviews*, 2012, vol. 64, no. 2, pp. 190-199. ISSN 0169-409X.

[8] HAUCK, T. S. et al. Assessing the Effect of Surface Chemistry on Gold Nanorod Uptake, Toxicity, and Gene Expression in Mammalian Cells. *Small*, 2008, vol. 4, no. 1, pp. 153-159. ISSN 1613-6829.

[9] LEE, S. et al. Rapid and selective separation for mixed proteins with thiol functionalized magnetic nanoparticles. *Nanoscale Research Letters*, 2012, vol. 7, no. 1, pp. 279. ISSN 1556-276X.

[10] FRASCONI, M. et al. Protein immobilization at gold-thiol surfaces and poteinal for biosensing. *Anal Bioanal Chem*, 2010, vol. 398, pp. 1545.

[11] MA ZHIYA, X. H., LIU YUPING, LIU BO, CHEN WEI, ZHAO YUANDI Applications of gold nanorods in biomedical imaging and related fields. *Chinese Science Bulletin*, 2013, vol. 58, no. 21, pp. 2530-2536.

[12] MA, Z. et al. Applications of gold nanorods in biomedical imaging and related fields. *Chinese Science Bulletin*, 2013, vol. 58, no. 21, pp. 2530-2536. ISSN 1001-6538.

[13] MIN, Y. et al. Gold nanorods for platinum based prodrug delivery. *Chemical Communications*, 2010, vol. 46, no. 44, pp. 8424-8426. ISSN 1359-7345.

[14] Conference ProceedingsHOMOLA, J. et al. *Surface plasmon resonance sensors using optical waveguides*. 10.1117/12.284728.

[15] LEE, G.-J. et al. Preparation of silver nanorods through the control of temperature and pH of reaction medium. *Materials Chemistry and Physics*, 2004, vol. 84, no. 2–3, pp. 197-204. ISSN 0254-0584.

[16] SRIRAJASKANTHAN, R. a PREEDY, V. R. *Nanomedicine and Cancer*. Science Publishers, 2011. pp. ISBN 9781578087273.

[17] NEHL, C. L. a HAFNER, J. H. Shape-dependent plasmon resonances of gold nanoparticles. *Journal of Materials Chemistry*, 2008, vol. 18, no. 21, pp. 2415-2419. ISSN 0959-9428.

[18] NOVO, C. et al. Direct observation of chemical reactions on single gold nanocrystals using surface plasmon spectroscopy. *Nat Nanotechnol*, 2008, vol. 3, no. 10, pp. 598-602. ISSN 1748-3387.

[19] ZOU, R. et al. Thermal stability of gold nanorods in an aqueous solution. *Colloids and Surfaces A: Physicochemical and Engineering Aspects*, 2010, vol. 372, no. 1–3, pp. 177-181. ISSN 0927-7757.
[20] HUANG, X. et al. Plasmonic photothermal therapy (PPTT) using gold nanoparticles. *Lasers in Medical Science*, 2008, vol. 23, no. 3, pp. 217-228. ISSN 0268-8921.
[21] JANA, N. R. et al. Seed-Mediated Growth Approach for Shape-Controlled Synthesis of Spheroidal and Rod-like Gold Nanoparticles Using a Surfactant Template. *Advanced Materials*, 2001, vol. 13, no. 18, pp. 1389-1393. ISSN 1521-4095.
[22] ALI, M. R. K. et al. Synthesis and Optical Properties of Small Au Nanorods Using a Seedless Growth Technique. *Langmuir*, 2012, vol. 28, no. 25, pp. 9807-9815. ISSN 0743-7463.
[23] LINK, S. a EL-SAYED, M. A. Size and Temperature Dependence of the Plasmon Absorption of Colloidal Gold Nanoparticles. *The Journal of Physical Chemistry B*, 1999, vol. 103, no. 21, pp. 4212-4217. ISSN 1520-6106.
[24] TAKENAKA, Y. et al. Effects of surfactant concentration on formation of high-aspect-ratio gold nanorods. *Journal of Colloid and Interface Science*, 2013, vol. 407, no. 0, pp. 265-272. ISSN 0021-9797.
[25] TOMA, H. E. et al. The coordination chemistry at gold nanoparticles. *Journal of the Brazilian Chemical Society*, 2010, vol. 21, pp. 1158-1176. ISSN 0103-5053.
[26] TSVETKOV, M. Y. et al. SERS substrates formed by gold nanorods deposited on colloidal silica films. *Nanoscale Research Letters*, 2013, vol. 8, no. 1, pp. 250. ISSN 1556-276X.
[27] ZIJLSTRA, P. et al. Optical detection of single non-absorbing molecules using the surface plasmon resonance of a gold nanorod. *Nat Nano*, 2012, vol. 7, no. 6, pp. 379-382. ISSN 1748-3387.
[28] GORMLEY, A. J. et al. Gold nanorod mediated plasmonic photothermal therapy: A tool to enhance macromolecular delivery. *International Journal of Pharmaceutics*, 2011, vol. 415, no. 1–2, pp. 315-318. ISSN 0378-5173.
[29] AMIJI, M. M. The Handbook of Nanomedicine. By Kewal K. Jain. *ChemMedChem*, 2008, vol. 3, no. 12, pp. 1977-1977. ISSN 1860-7187.
[30] ZHAROV, V. P. et al. Photothermal Nanotherapeutics and Nanodiagnostics for Selective Killing of Bacteria Targeted with Gold Nanoparticles. *Biophysical Journal*, 2006, vol. 90, no. 2, pp. 619-627. ISSN 0006-3495.
[31] EKICI, O. et al. Thermal analysis of gold nanorods heated with femtosecond laser pulses. *Journal of Physics D: Applied Physics*, 2008, vol. 41, no. 18, pp. 185501. ISSN 0022-3727.
[32] LINK, S. a SAYED, E. Optical properties and ultrafast dynamics of metallic nanocrystals. *Annu. Rev. Phys. Chem.*, 2004, vol. 54, pp. 331.
[33] HUANG, X. et al. Cancer cell imaging and photothermal therapy in the near-infrared region by using gold nanorods. *J Am Chem Soc*, 2006, vol. 128, no. 6, pp. 2115-2120. ISSN 0002-7863 (Print)0002-7863 (Linking).
[34] NHIEM, T. a THOMAS, J. W. Understanding magnetic nanoparticle osteoblast receptor-mediated endocytosis using experiments and modeling. *Nanotechnology*, 2013, vol. 24, no. 18, pp. 185102. ISSN 0957-4484.
[35] OKUNO, T. et al. Photothermal therapy of tumors in lymph nodes using gold nanorods and near-infrared laser light. *Journal of Controlled Release*, 2013, vol. 172, no. 3, pp. 879-884. ISSN 0168-3659.
[36] O'NEAL, D. P. et al. Photo-thermal tumor ablation in mice using near infrared-absorbing nanoparticles. *Cancer Letters*, 2004, vol. 209, no. 2, pp. 171-176. ISSN 0304-3835.

[37] HUANG, X. et al. Cancer Cell Imaging and Photothermal Therapy in the Near-Infrared Region by Using Gold Nanorods. *Journal of the American Chemical Society*, 2006, vol. 128, no. 6, pp. 2115-2120. ISSN 0002-7863.
[38] HUANG, X. et al. Gold Nanorods: From Synthesis and Properties to Biological and Biomedical Applications. *Advanced Materials*, 2009, vol. 21, no. 48, pp. 4880-4910. ISSN 1521-4095.
[39] NIKOOBAKHT, B. a EL-SAYED, M. A. Preparation and Growth Mechanism of Gold Nanorods (NRs) Using Seed-Mediated Growth Method. *Chemistry of Materials*, 2003, vol. 15, no. 10, pp. 1957-1962. ISSN 0897-4756.
[40] JIANG, X. C. et al. Gold nanorods: Limitations on their synthesis and optical properties. *Colloids and Surfaces A: Physicochemical and Engineering Aspects*, 2006, vol. 277, no. 1–3, pp. 201-206. ISSN 0927-7757.
[41] NIKOOBAKHT, B. a EL-SAYED, M. A. Evidence for Bilayer Assembly of Cationic Surfactants on the Surface of Gold Nanorods. *Langmuir*, 2001, vol. 17, no. 20, pp. 6368-6374. ISSN 0743-7463.
[42] NARAYANAN, K. B. a SAKTHIVEL, N. Green synthesis of biogenic metal nanoparticles by terrestrial and aquatic phototrophic and heterotrophic eukaryotes and biocompatible agents. *Advances in Colloid and Interface Science*, 2011, vol. 169, no. 2, pp. 59-79. ISSN 0001-8686.
[43] NADAGOUDA, M. N. a VARMA, R. S. Green and controlled synthesis of gold and platinum nanomaterials using vitamin B2: density-assisted self-assembly of nanospheres, wires and rods. *Green Chemistry*, 2006, vol. 8, no. 6, pp. 516-518. ISSN 1463-9262.
[44] ISAAC, R. S. R. et al. Green Synthesis of Gold and Silver Nanoparticles Using Averrhoa bilimbi Fruit Extract. *Journal of Nanotechnology*, 2013, vol. 2013, pp. 6.
[45] PÉREZ-JUSTE, J. et al. Electric-Field-Directed Growth of Gold Nanorods in Aqueous Surfactant Solutions. *Advanced Functional Materials*, 2004, vol. 14, no. 6, pp. 571-579. ISSN 1616-3028.
[46] NIKOOBAKHT, B. a EL-SAYED, M. Preparation and growth mechanism of gold nanorods (NRs) using seed-mediated growth method. *Chem Mater*, 2003, vol. 15, pp. 1957 - 1962.
[47] BECKER, R. et al. CTAB promoted synthesis of Au nanorods – Temperature effects and stability considerations. *Journal of Colloid and Interface Science*, 2010, vol. 343, no. 1, pp. 25-30. ISSN 0021-9797.
[48] SMITH, D. K. a KORGEL, B. A. The Importance of the CTAB Surfactant on the Colloidal Seed-Mediated Synthesis of Gold Nanorods. *Langmuir*, 2008, vol. 24, no. 3, pp. 644-649. ISSN 0743-7463.
[49] PATEL, V. et al. pH controlled size/shape in CTAB micelles with solubilized polar additives: A viscometry, scattering and spectral evaluation. *Colloids and Surfaces A: Physicochemical and Engineering Aspects*, 2014, vol. 455, no. 0, pp. 67-75. ISSN 0927-7757.
[50] ORENDORFF, C. J. et al. pH-Triggered Assembly of Gold Nanorods. *Langmuir*, 2005, vol. 21, no. 5, pp. 2022-2026. ISSN 0743-7463.
[51] VIGDERMAN, L. et al. Quantitative Replacement of Cetyl Trimethylammonium Bromide by Cationic Thiol Ligands on the Surface of Gold Nanorods and Their Extremely Large Uptake by Cancer Cells. *Angewandte Chemie International Edition*, 2012, vol. 51, no. 3, pp. 636-641. ISSN 1521-3773.
[52] BUSBEE, B. D. et al. An Improved Synthesis of High-Aspect-Ratio Gold Nanorods. *Advanced Materials*, 2003, vol. 15, no. 5, pp. 414-416. ISSN 1521-4095.

[53] DE LA MORA, M. B. et al. Porous silicon photoluminescence modification by colloidal gold nanoparticles: Plasmonic, surface and porosity roles. *Journal of Luminescence*, 2014, vol. 146, no. 0, pp. 247-255. ISSN 0022-2313.
[54] SHEN, S. et al. Targeting mesoporous silica-encapsulated gold nanorods for chemo-photothermal therapy with near-infrared radiation. *Biomaterials*, 2013, vol. 34, no. 12, pp. 3150-3158. ISSN 0142-9612.
[55] VIGDERMAN, L. et al. Functional Gold Nanorods: Functional Gold Nanorods: Synthesis, Self-Assembly, and Sensing Applications (Adv. Mater. 36/2012). *Advanced Materials*, 2012, vol. 24, no. 36, pp. 5016-5016. ISSN 1521-4095.
[56] ZHAO, W. a KARP, J. M. Tumour targeting: Nanoantennas heat up. *Nat Mater*, 2009, vol. 8, no. 6, pp. 453-454. ISSN 1476-1122.
[57] WANG, J. et al. Glutathione modified gold nanorods with excellent biocompatibility and weak protein adsorption, targeting imaging and therapy toward tumor cells. *Dalton Transactions*, 2013, vol. 42, no. 32, pp. 11548-11558. ISSN 1477-9226.
[58] HUANG, H. et al. Preparation and optical properties of worm-like gold nanorods. *Journal of Colloid and Interface Science*, 2008, vol. 322, no. 1, pp. 136-142. ISSN 0021-9797.
[59] HUANG, P. et al. Folic acid-conjugated Silica-modified gold nanorods for X-ray/CT imaging-guided dual-mode radiation and photo-thermal therapy. *Biomaterials*, 2011, vol. 32, no. 36, pp. 9796-9809. ISSN 0142-9612.
[60] ZHANG, Z. et al. Mesoporous Silica-Coated Gold Nanorods as a Light-Mediated Multifunctional Theranostic Platform for Cancer Treatment. *Advanced Materials*, 2012, vol. 24, no. 11, pp. 1418-1423. ISSN 1521-4095.
[61] YANG, X. et al. Near-Infrared Light-Triggered, Targeted Drug Delivery to Cancer Cells by Aptamer Gated Nanovehicles. *Advanced Materials*, 2012, vol. 24, no. 21, pp. 2890-2895. ISSN 1521-4095.
[62] LIOPO, A. V. et al. Highly purified biocompatible gold nanorods for contrasted optoacoustic imaging. *Nanosci Nanotechnol Lett*, 2012, vol. 4, no. 7, pp. 681-686. ISSN 1941-4900 (Print)1941-4900 (Linking).
[63] GARABAGIU, S. a BRATU, I. Thiol containing carboxylic acids remove the CTAB surfactant onto the surface of gold nanorods: An FTIR spectroscopic study. *Applied Surface Science*, 2013, vol. 284, no. 0, pp. 780-783. ISSN 0169-4332.
[64] Conference ProceedingsLIOPO, A. V. et al. *PEG-coated gold nanorod monoclonal antibody conjugates in preclinical research with optoacoustic tomography, photothermal therapy, and sensing*. 10.1117/12.910838.
[65] MANSON, J. et al. Polyethylene glycol functionalized gold nanoparticles: the influence of capping density on stability in various media. *Gold Bulletin*, 2011, vol. 44, no. 2, pp. 99-105.
[66] LIOPO, A. V. et al. Laser nanothermolysis of human leukemia cells using functionalized plasmonic nanoparticles, no. 2150-5578 (Print).
[67] RAJA, G. R. et al. In vitro toxicity studies of polymer-coated gold nanorods. *Nanotechnology*, 2010, vol. 21, no. 14, pp. 145101. ISSN 0957-4484.
[68] GOMEZ, L. et al. Stability and biocompatibility of photothermal gold nanorods after lyophilization and sterilization. *Materials Research Bulletin*, 2013, vol. 48, no. 10, pp. 4051-4057. ISSN 0025-5408.
[69] LIU, X. S. et al. Surface and Size Effects on Cell Interaction of Gold Nanoparticles with Both Phagocytic and Nonphagocytic Cells. *Langmuir*, 2013, vol. 29, no. 29, pp. 9138-9148. ISSN 0743-7463.
[70] RISS TL, M. R., NILES ALET. Cell Viability Assays. *Assay Guidance Manual* 2013. Available from:<http://www.ncbi.nlm.nih.gov/books/NBK144065/>.

[71] DANILATOS, G. D. a ROBINSON, V. N. E. Principles of scanning electron microscopy at high specimen chamber pressures. *Scanning*, 1979, vol. 2, no. 2, pp. 72-82. ISSN 1932-8745.
[72] ZHANG, B. a SU, D. S. Transmission Electron Microscopy and the Science of Carbon Nanomaterials. *Small*, 2013, pp. n/a-n/a. ISSN 1613-6829.
[73] YU, Z. et al. Utilizing Dynamic Light Scattering as a Process Analytical Technology for Protein Folding and Aggregation Monitoring in Vaccine Manufacturing. *Journal of Pharmaceutical Sciences*, 2013, vol. 102, no. 12, pp. 4284-4290. ISSN 1520-6017.
[74] HAMON, C. et al. Replacement of CTAB with peptidic ligands at the surface of gold nanorods and their self-assembling properties. *Journal of Colloid and Interface Science*, 2014, vol. 424, no. 0, pp. 90-97. ISSN 0021-9797.
[75] PARK, S. et al. Effective Size and Zeta Potential of Nanorods by Ferguson Analysis. *Langmuir*, 2010, vol. 26, no. 16, pp. 13071-13075. ISSN 0743-7463.
[76] DOUGHERTY, G. M. et al. The zeta potential of surface-functionalized metallic nanorod particles in aqueous solution, no. 0173-0835 (Print).
[77] VONNEMANN, J. et al. Polyglycerolsulfate functionalized gold nanorods as optoacoustic signal nanoamplifiers for in vivo bioimaging of rheumatoid arthritis. *Theranostics*, 2014, vol. 4, no. 6, pp. 629-641.
[78] CONVERSANO, F. et al. Echographic detectability of optoacoustic signals from low-concentration PEG-coated gold nanorods. *International Journal of Nanomedicine*, 2012, vol. 7, pp. 4373-4389. ISSN 1178-2013.
[79] LIU, F.-K. Using Size-Exclusion Chromatography to Monitor Variations in the Sizes of Microwave-Irradiated Gold Nanoparticles. *ISRN Chromatography*, 2012, vol. 2012, pp. 7.